CALCULATING SOLAR PHOTOVOLTAIC POTENTIAL ON RESIDENTIAL ROOFTOPS IN KAILUA KONA, HAWAII

By

Caroline Carl

A Thesis Presented to the
FACULTY OF THE USC GRADUATE SCHOOL
UNIVERSITY OF SOUTHERN CALIFORNIA
In Partial Fulfillment of the
Requirements for the Degree
MASTER OF SCIENCE
GEOGRAPHIC INFORMATION SCIENCE AND TECHNOLOGY

May 2014

ACKNOWLEDGEMENTS

I would like to thank my loving husband Bill and beautiful baby girl Delainey for all their support throughout this entire process. Without their patience, I could never have completed this work.

I would also like to thank Professor Su Jin Lee for guiding me through this process and always going above and beyond. Thank you for taking on this work with me, which has been the greatest learning experience of my life.

TABLE OF CONTENTS

ACKNOWLEDGEMENTS ii

LIST OF FIGURES vi

LIST OF EQUATIONS vii

LIST OF TABLES viii

ABSTRACT ix

CHAPTER 1: INTRODUCTION 1

1.1 Renewable Energy and Trends in Solar Photovoltaic Energy Production 1

1.2 Electricity Demand in Hawaii 4

1.3 Growth of Solar Photovoltaic in Hawaii 5

1.4 Solar Photovoltaic Research on Hawaii Island 7

CHAPTER 2: LITERATURE REVIEW 10

2.1 Modeling Solar Radiation 10

2.2 Solar Radiation Models with GIS 12

2.2.1 Esri's Solar Analyst 14

2.3 Calculating Rooftop Area 17

2.4 Calculating Photovoltaic Potential from Solar Radiation 19

2.5 Solar Mapping Projects as Decision Support Tools 23

2.6 Hawaii Solar Mapping Projects 24

2.6.1 Oahu 24

2.6.2 Kauai 26

2.6.3 Hawaii Island 27

2.6.4 Statewide 27

CHAPTER 3: METHODS 29

3.1 Description of Study Area 29

3.2 Data 30

3.2.1 LiDAR data 30

3.2.2 Tax Map Key Parcel Data 32

3.2.3 Aerial Imagery 33

3.2.4 PV Production on Active Residential Site 33

3.3 Research Design 34

3.3.1 Isolating Building Rooftops for Sample Set 36

3.3.1.1 Stratified Parcel Selection 36

3.3.1.2 Digitizing Rooftops 38

3.3.2 Estimating Terrain Parameters and Incoming Solar Radiation 39

3.3.2.1 Terrain Parameters: Slope and Aspect 39

3.3.2.2 Estimating Solar Radiation 40

3.3.3 Spatial Analysis for Selected Rooftops 44

3.3.3.1 Raster to Point 44

3.3.3.2 Spatial Join 47

3.3.4 Calculating PV Potential on Building Rooftops 49

3.3.5 Statistical Analysis for Extrapolation to Study Area 50

CHAPTER 4: RESULTS 52

4.1 Distribution of Lot Sizes, Rooftop Area, Terrain Parameters, and PV Potential 52

4.2 Correlation Analysis 54

4.3 Rooftop and Lot Size Correlation 58

4.4 Regression Analysis 59

4.5 Extrapolation to Study Area: Rooftop Area, Average and Total PV Potential 61

4.6 Comparison with Real Home PV Production 63

CHAPTER 5: CONCLUSION AND DISCUSSION 66

5.1 Project Assumptions 68

5.2 Review of Methodology 70

5.2.1 LiDAR Performance 70

5.2.2 Modeling Solar Radiation 71

5.2.3 Rooftop Area Estimation 72

5.2.4 Estimating PV Potential 73

5.3 Future research 74

5.3.1 LiDAR 75

5.3.2 Optimizing Solar Radiation Model 76

REFERENCES 77

LIST OF FIGURES

Figure 1.1 Breakdown of electric energy sources in Hawaii 4

Figure 2.1 Incoming solar radiation components 10

Figure 3.1 Study area LiDAR coverage 30

Figure 3.2 Elevation with 2-meter spatial resolution from LiDAR 32

Figure 3.3 Flowchart for calculating PV potential for this study 35

Figure 3.4 Sample set of rooftops 38

Figure 3.5 Map showing aspect 39

Figure 3.6 Map showing slope 40

Figure 3.7 Incoming solar radiation surface 43

Figure 3.8 Points of solar radiation on rooftops 45

Figure 3.9 Aspect points on rooftop 46

Figure 3.10 High resolution sample rooftop image from Google Earth 46

LIST OF EQUATIONS

Equation 1: Suri et al. photovoltaic potential calculation 20

Equation 2: Hofierka and Kanuk photovoltaic potential 21

Equation 3: Jakubiec and Reinhart 2012 22

Equation 4: Jakubiec and Reinhart 2012 adapted from NREL PVWatts Version 2 22

LIST OF TABLES

Table 3.1 Tax map key (TMK) parcel data attributes 33

Table 3.2 Stratified parcel selection 37

Table 3.3 Samples design for digitization 38

Table 3.4 Input parameters for area solar radiation tool in ArcGIS 42

Table 3.5 Final rooftop layer attribute table used for PV potential calculation 48

Table 3.6 PV potential calculated data for rooftop layer attribute table 50

Table 4.1 Statistical summary of sample set parcel attributes in six classes 53

Table 4.2 Standard correlation showing the relationship between variables across all classes 55

Table 4.3 Standard correlation table showing the relationship between variables across all 224 samples 57

Table 4.4 Bivariate fit modeling the correlation between rooftop and lot size for each class 1-6 and the total sample set 58

Table 4.5 Average PV potential least squares regression analysis 59

Table 4.6 Total PV potential least squares regression analysis 60

Table 4.7 Regression analysis average and total PV potential 62

Table 4.8 Solar panel information used for model versus as built in sample home 61

Table 4.9 Recorded PV production data compared with adjusted model 65

ABSTRACT

As carbon based fossil fuels become increasingly scarce, renewable energy sources are coming to the forefront of policy discussions around the globe. As a result, the State of Hawaii has implemented aggressive goals to achieve energy independence by 2030. Renewable electricity generation using solar photovoltaic technologies plays an important role in these efforts. This study utilizes geographic information systems (GIS) and Light Detection and Ranging (LiDAR) data with statistical analysis to identify how much solar photovoltaic potential exists for residential rooftops in the town of Kailua Kona on Hawaii Island. This study helps to quantify the magnitude of possible solar photovoltaic (PV) potential for Solar World SW260 monocrystalline panels on residential rooftops within the study area.

Three main areas were addressed in the execution of this research: (1) modeling solar radiation, (2) estimating available rooftop area, and (3) calculating PV potential from incoming solar radiation. High resolution LiDAR data and Esri's solar modeling tools and were utilized to calculate incoming solar radiation on a sample set of digitized rooftops. Photovoltaic potential for the sample set was then calculated with the equations developed by Suri et al. (2005). Sample set rooftops were analyzed using a statistical model to identify the correlation between rooftop area and lot size. Least squares multiple linear regression analysis was performed to identify the influence of slope, elevation, rooftop area, and lot size on the modeled PV potential values. The equations built from these statistical analyses of the sample set were applied to the entire study region to calculate total rooftop area and PV potential.

The total study area statistical analysis findings estimate photovoltaic electric energy generation potential for rooftops is approximately 190,000,000 kWh annually. This is approximately 17 percent of the total electricity the utility provided to the entire island in 2012. Based on these findings, full rooftop PV installations on the 4,460 study area homes could provide enough energy to power over 31,000 homes annually.

The methods developed here suggest a means to calculate rooftop area and PV potential in a region with limited available data. The use of LiDAR point data offers a major opportunity for future research in both automating rooftop inventories and calculating incoming solar radiation and PV potential for homeowners.

CHAPTER 1: INTRODUCTION

1.1 Renewable Energy and Trends in Solar Photovoltaic Energy Production

Around the globe, concern is mounting over conventional carbon based energy production. The issues at hand are numerous and include increasing atmospheric carbon dioxide concentrations from greenhouse gas emissions, environmental safety of energy production techniques, volatile energy prices, and depleting carbon based fuel reserves to name a few (Nguyen and Pearce 2010; Choi et al. 2011). As a result, countries are facing an increasing challenge to diversify energy sources and bringing renewable generation to the forefront of policy discussion.

In the United States, a rise in renewable energy generation has been supported by the availability of federal tax credits and programs in individual states (U.S. Energy Information Administration 2013a). Many states are implementing renewable portfolio standards, or renewable energy standards, that outline goals to increase electricity generation from renewable resources (U.S. Energy Information Administration 2013a). These policies seek to remove barriers to install renewable generation and can include grant programs, loan programs, and state renewable electricity tax credits. The Database of State Incentives for Renewables & Efficiency (DSIRE) provides an outline of state renewable portfolio standards available throughout the nation (North Carolina State University 2013).

In 2012, about 12 percent of U.S. electricity was generated from renewable sources (U.S. Energy Information Administration 2013b). The United States Energy Information Administration states that the five renewable sources most often utilized include biomass, water, geothermal, wind and solar (U.S. Energy Information

Administration 2013b). Of these, hydropower (water) contributed 7 percent of renewable electricity generation (U.S. Energy Information Administration 2013c). The other common renewable sources make up the remaining 5 percent including wind (3.46 percent), biomass (1.42 percent), geothermal (0.41 percent), and solar (0.11 percent) (U.S. Energy Information Administration 2013c). The study presented in this manuscript focuses on renewable generation from solar energy.

Solar energy is received from the sun's light rays hitting the earth and is commonly referred to as solar radiation (U.S. Energy Information Administration 2013d). Solar radiation can be harnessed and converted to electricity by photovoltaic (PV) technologies. Photovoltaic cells produce electricity by absorbing photons and releasing electrons that can be captured in the form of an electric current (Knier 2011). Cells can be used individually to power small electronics or grouped together into modules and arrays to generate larger amounts of power (U.S. Energy Information Administration 2013d). PV array systems are becoming an increasingly popular means for powering residential and commercial locations in the form of distributed generation (Loudat 2013).

The photovoltaic market in the United States has grown tremendously in the last decade (U.S. Energy Information Administration 2013a). PV is a robust technology that possesses a great deal of potential because it is both scalable and geographically dispersed (Pearce 2002; Zekai 2004; Nguyen and Pearce 2010; Choi et al. 2011). In an article in Renewable Energy Focus, Dianna Herbst (2009) explains how PV production has been doubling every two years, increasing by an average of 48 percent each year since 2002, making it the world's fastest growing energy technology. In 2012, PV

technology consisted of 12 percent of all new U.S. electricity generation (Interstate Renewable Energy Council (IREC) 2013).

Despite a banner year for solar technologies in 2012, it only comprises 0.11 percent of overall electricity generation in the United States and many barriers to the wide scale adoption of photovoltaic production still exist (U.S. Energy Information Administration 2013c). Initial cost is a major barrier to implementation of PV systems (Súri and Hofierka 2004). Even with falling prices, renewable sources of energy are still expensive compared to traditional fossil fuel generation. The expense of installation and lack of information to quantify PV technology capacity, and thus predicting return on investment, are a few of the barriers facing the industry today (Choi et al. 2011; Herbst 2012). Beyond financial factors there are a number of social and regulatory factors that can influence a consumer's decision to purchase solar panels.

In addition to existing renewable portfolio standards and tax credits, many state, city and local governments to break down barriers for distributed PV installation have implemented GIS-based modeling and decision support tools (Voivontas, Assimacopolous and Mourelatos 1998). Online solar potential maps are one type of decision support tool that is becoming increasingly popular throughout cities in the United States. Currently cities such as Boston, Denver, New York, Portland, San Diego, and San Francisco host online solar potential mapping sites available to the public. These allow users to evaluate the geographical, technological and financial factors that affect system performance and then predict the costs and benefits associated with installing solar PV panels for both residential and commercial buildings.

1.2 Electricity Demand in Hawaii

The economic consequences of fossil fuel dependence are profound in Hawaii. Figure 1.1 outlines the breakdown of electric energy sources as of February 2013 (U.S. EIA 2013e). The state relies on petroleum for 73 percent of its electricity generation and, with no indigenous fossil fuel resources like oil or coal, Hawaii must import the majority of its energy resources (Piwko, et al. 2012; State of Hawaii Department of Business, Economic Development and Tourism (DBEDT) 2013a). The island chain is located over 2,500 miles from any major land mass which greatly increases the cost of transport and translates into electricity rates that are three times greater than the U.S. average (Piwko et al. 2012; DBEDT 2013a; U.S. EIA 2013e).

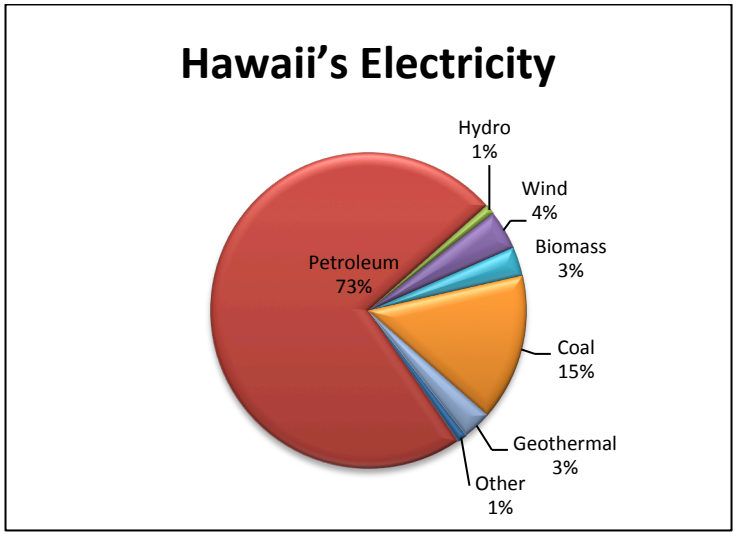

Figure 1.1 Breakdown of electric energy sources in Hawaii
(*Source: Electric Power Monthly, U.S. EIA 2013e)*

Despite the state's dependence on imported oil, there simultaneously exists an abundance of renewable energy generation sources including geothermal, ocean power, wind, and sunshine. To harness these, the state has one of the most aggressive clean energy goals in the nation. The Hawaii Clean Energy Initiative (HCEI) was launched in

2008, when the governor of the State of Hawaii and the U.S. Department of Energy signed a historic agreement committing the state to achieve 70 percent clean energy by 2030 (HCEI 2010). This 70 percent will be comprised of 30 percent energy efficiency and 40 percent generation from local renewable sources (HCEI 2010). Various scenarios for achieving this goal have been proposed by several working groups comprised of local stakeholders and national experts. The HCEI remains an ongoing, collaborative effort within which rooftop solar generation plays a significant role in the path to achieving energy independence in the State of Hawaii (HCEI 2011).

A number of documents produced by the Hawaii Clean Energy Initiative and the State of Hawaii Department of Business and Economic Development (DBEDT) reference the importance of increasing solar generation capacity in order to meet renewable energy goals (Global Energy Concepts 2006; Braccio, Finch and Frazier 2012). In an analysis of the Hawaii Clean Energy Initiative End State 2030 Scenarios, estimates for installed capacity for residential rooftop solar ranged between 67-205 Megawatts (MW) (Braccio et al. 2012). The most ideal end state scenario suggested by the working group proposes 179 MW of residential rooftop solar by the year 2030 (Braccio et al. 2012).

1.3 Growth of Solar Photovoltaic in Hawaii

In the five years since the Hawaii Clean Energy Initiative was enacted, solar generation has seen unprecedented growth. The United States Energy Information Administration (2012) states that solar PV capacity increased by 150 percent in 2011, making it the eleventh largest state for PV capacity. In 2012 the growth rate was 182 percent moving it up to the seventh slot (DBEDT 2013a; IREC 2013). In a recent publication of Hawaii Energy Facts and Figures, DBEDT states the 2013 installed

capacity for distributed PV at 223 MW. Residential rooftops represent 28,351 systems contribute 57 percent of this total or approximately 127 MW (DBEDT 2013a).

This growth can be attributed to a combination of falling prices, federal and state solar tax credits, and increased use of leases with third party ownership for systems (IREC 2013). Financial incentives work for the solar industry by lowering the cost of panels thus enhancing the affordably of solar photovoltaic systems for both residential and commercial buildings (Kerschen 2012). A recent study performed by the Blue Planet Foundation explains how Hawaii's solar tax credit has been extremely effective at making the state a leader in both PV and solar water heating (Loudat 2013). Based on these trends, one might think there is no need to assess overall PV potential as Hawaii will continue to witness exponential growth as they march towards their clean energy goals. This may not, however, be the case for long.

The majority of PV systems in Hawaii are net energy metered (DBEDT 2013a). Net energy metering gives residential and commercial customers the ability to feed excess solar energy to the utility grid and receive full retail value to offset the electricity supplied to them by the utility (Hawaii Electric Company (HECO) 2013). Each distribution circuit has specific penetration levels of non-firm solar power that are deemed acceptable in order to ensure reliable service on that circuit (HECO 2013). High penetration of residential and commercial distributed generation from solar thus brings additional concerns regarding interconnection and grid saturation (Mangelsdorf 2013a, 2013b and 2013c; IREC 2013).

Each of the main islands has an independent electricity grid. Because there are no interconnections between islands there is a critical risk of grid saturation (Piwko et al.

2012; DBEDT 2013a). The Hawaii Electric Company serving Oahu and its subsidiaries, Maui Electric Company (MECO) serving the county of Maui (Maui, Lanai and Molokai) and Hawaii Electric Light Company, Inc. (HELCO) serving Hawaii Island, maintain that circuits with distributed generation capacity less than 15 percent peak load may qualify for simple interconnection (HECO 2013). For those over 15 percent, further investigation may be necessary before systems can be added. Each utility maintains its own maps that allow customers to view a summary of distributed generation peak load by circuit (HECO 2013).

At the time this project research was being conducted, circuit saturation was a critical issue. One just need peruse the local newspapers to see references to solar 'feeding frenzy' and solar market consolidation (Mangelsdorf 2013a, 2013b and 2013c). As of September 2013, HECO and its subsidiaries issued an update asking all customers to receive approval prior to any installation moving forward (HECO 2013; HELCO 2013; and MECO 2013). This has slowed the interconnection process spurring outrage from many customers waiting to connect their recently installed solar PV systems.

1.4 Solar Photovoltaic Research on Hawaii Island

It is important to note that while the Hawaii Clean Energy Initiative is a statewide effort, each county has its own clean energy initiatives that inform the steering committee at the state level (HCEI 2011). Each county has its own unique demographic and environmental characteristics that influence renewable generation capacity. The work discussed in this paper focuses on Hawaii Island, commonly referred to as the "Big Island," as it is the largest and youngest island within the Hawaiian archipelago. The total population of Hawaii Island is a little over 185,000 and the population density is

relatively low at about 46 people per square mile. The area chosen for evaluation in this study lies on the leeward side of the island in the town of Kailua Kona. It is approximately 628 Km^2 and extends about 44 kilometers north to south over Kailua Kona.

Hawaii Island is serviced by the Hawaii Electric Light Company, Inc. (HELCO). The utility has a total generating capacity of 359 MW and experiences a system peak of 189 MW (HELCO 2013). In 2012 HELCO provided 1,085 Gigawatt-hours (GWh) of electricity to the Big Island (DBEDT 2013a). Residential customers utilized 38 percent of this energy, or 412.3 GWh (DBEDT 2013a). In June 2013, DBEDT listed the total number of PV systems for the Big Island at 3,913 with a capacity of 28.9 MW. Of these an estimated 92 percent, or approximately 3,600, are residential. These residential PV systems have a total capacity of 15.84 MW (DBEDT 2013a).

Much like the rest of the state, Hawaii Island residents are seeing the effects of circuit saturation associated with distributed PV generation. In the face of growing uncertainty, it seems more important than ever for residents to understand the total solar photovoltaic potential on their rooftops based on their location and the factors that affect PV performance before making a significant investment in this technology. To date, investigation into the future PV generation potential on the Island of Hawaii has not been as common as it has been elsewhere. In one study produced in 2007 by The Kohala Center, an independent research institute, HELCO estimates that with the continued subsidies installed solar generating capacity on the Big Island could be between 80-130 MW by 2030 (Davies et al.2007). Beyond this, little else could be found regarding the total distributed PV generation potential for this Island.

The research presented in this study utilizes the modeling and analytical power of geographic information systems (GIS) with statistical analysis to answer the question: *What is the solar PV potential of residential rooftops in the town of Kailua Kona on Hawaii Island?* The study calculates total PV potential for a sample set using Esri's solar radiation modeling tools and existing PV equations. It then uses statistical analysis to extrapolate the findings to the entire study area.

While a number of solar PV mapping initiatives exist throughout world, this research will be the first study of its type on the Big Island. It is an effort to quantify the magnitude of possible solar PV electric energy generation on residential rooftops within the specific study area. The hope is that this can be a launching point for future studies using LiDAR data to evaluate rooftop solar potential.

The next chapter includes a review of existing literature that pertains to the goal of this study. Three main areas were addressed in the execution of this research: (1) modeling solar radiation, (2) estimating available rooftop area, and (3) calculating PV potential from incoming solar radiation. The literature review also includes a discussion of existing solar mapping efforts. The material discussed in the literature review was used to inform the methods chosen for this study. The remaining chapters 3, 4, and 5 outline the methodology, results and conclusions for the work completed.

CHAPTER 2: LITERATURE REVIEW

The potential for photovoltaic electricity generation on rooftops depends on a number of global, local, temporal, and spatially variable conditions (Redweik, Catita, and Brito 2011). The literature review included here discusses the factors that influence PV potential including incoming solar radiation, available rooftop area, and the effects of panel efficiency. Section 2.1 and 2.2 discuss existing methods for modeling incoming solar radiation with GIS, Section 2.3 discusses rooftop calculation methods and Section 2.4 addresses methods for calculating photovoltaic potential from solar radiation. The chapter concludes with a review of solar mapping initiatives in Hawaii.

2.1 Modeling Solar Radiation

It can be argued that the most important factor influencing photovoltaic electricity generation is the amount of incoming solar radiation. Solar radiation, or insolation, is the sun's energy reaching the earth's surface. It is comprised of three components: direct beam, diffuse, and ground-reflected radiation (Perez et al. 1987). Figure 2.1 displays the way the three components reach the earth's surface.

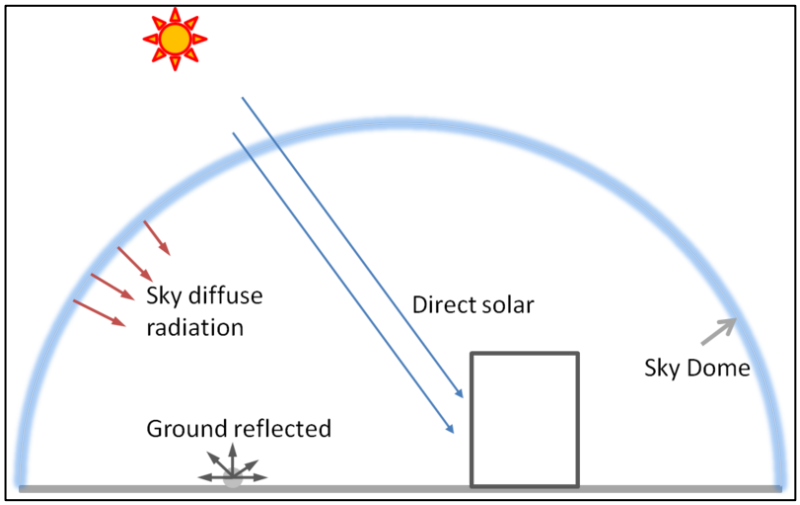

Figure 2.1 Incoming solar radiation components
(Source: International Building Performance Simulation Association 2011)

Direct radiation is the direct beam of solar energy that is intercepted by the surface without any interactions with particles in the atmosphere (Hetrick, Rich and Weiss 1993). Diffuse radiation is the intercepted radiation that is scattered in the atmosphere by gases and aerosols (Hetrick et al. 1993; Kumar, Skidmore and Knowles 1997). Reflected radiation is reflected from terrain and surrounding surfaces (Kumar et al. 1997, Esri 2013a). Together, direct, diffuse and reflected radiations make up global radiation, or total radiation, reaching the surface.

The amount of solar radiation reaching the surface depends on location, atmospheric effects, and topography. Solar radiation is affected by the earth's geometric rotation and revolution around the sun (Fu and Rich 1999). It also varies with environmental factors like atmospheric attenuation effects including cloud cover and water vapor (Fu and Rich 1999). On the ground, topographic effects such as elevation, slope, and orientation influence the amount of radiation reaching a surface (Kang, Kim and Lee 2002; Súri and Hofierka 2004).

Understanding the amount of solar radiation reaching a surface is important for more than just evaluating renewable energy potential. Almost all human activities depend on the sun's power (Fu and Rich 1999). Unfortunately, for most geographical areas, measured insolation data are incomplete or are available only at a very coarse scale (Fu and Rich 1999). Solar radiation data are measured at a number of ground stations around the world but because solar irradiation levels can vary drastically with the terrain, vegetation, ground structures and weather, in most cases it is not accurate to just use the nearest weather station in one's analysis. Studies have found that solar irradiance data

collected from stations 20-30 kilometers from a project can have a root mean square error as much as 25 percent (Perez, Seals and Zelenka 1997).

To overcome the scarcity of trustworthy measured solar radiation data, a number of empirical models have been developed to predict the amount of solar radiation reaching the earth's surface at a given point (Katiyar and Pandey 2013). These include those developed by Perez, Zhang, Kasten and Muneer (Seo 2010). Seo (2010) provides an extensive overview of existing empirical models developed to predict the intensity of solar radiation on the earth's surface. Clear sky models commonly use inputs such as solar angle, clearness index, beam and diffuse fraction, and average efficacy values in their calculations (Seo 2010). All-sky models are typically derived from clear sky models but consider additional variables like cloud cover and cloud layers in order to account for intermediate and overcast skies (Robinson and Stone 2004; Seo 2010). Despite the large number of models developed, no existing model is universally applicable. Models differ mainly in their consideration of the diffuse component of incoming radiation (Perez et al. 1987). This depends mostly on climate and regional terrain conditions (Súri and Hofierka 2004). In fact, most are developed and validated for a particular region (Seo 2010). The choice of model depends on the conditions in the area of study and the scale of analysis.

2.2 Solar Radiation Models with GIS

In the last two decades, several empirical solar radiation models have been enhanced by the use of geographic information systems tools. The faster processing capabilities associated with GIS platforms allows for integration of sophisticated solar radiation models and additional consideration of the effects of topography on incoming solar radiation (Dubayah and Rich 1995). GIS tools let the user examine the temporal and

spatial variability of incident solar radiation on a landscape level (Rich et al. 1994). Integrating solar radiation models within GIS has helped to eliminate the complexity of programming GIS functions into mathematical models (Nguyen and Pearce 2010). Moreover, solar radiation models with GIS can also incorporate environmental and socio-economic datasets for scenario modeling of interest to policy makers (Nguyen and Pearce 2010).

SolarFlux is one of the original GIS-based models (Súri and Hofierka 2004). It was implemented in the ARC/INFO platform as an ARC Macro Language (AML) program (Dubayah and Rich 1995). This tool simulates the influence of shadow patterns on direct insolation at specific intervals through time (Helios Environmental Modeling Institute, LLC 2000). It uses the input of a topographic surface with elevation values, latitude, time interval for calculation, and atmospheric conditions (Dubayah and Rich 1995). The output provided shows direct radiation flux, duration of direct radiation, skyview factor and diffuse radiation flux for each surface location (Dubayah and Rich 1995). While originally implemented at a variety of temporal and spatial scales, Súri and Hofierka (2004) explain how Solarflux uses simple empirical formulas wherein input parameters are averaged and therefore does not perform well when calculating over large areas.

The SRAD model calculates complex short-wave and long-wave interactions of solar energy with the earth's surface and atmosphere (Wilson and Gallant 2000; Súri and Hofierka 2004). The model is based on simplified underlying physics but incorporates the main solar radiation factors to account for the spatial variability of landscape processes (Sheng, Wilson and Lee 2009). It was designed to calculate solar radiation as a function

of latitude, slope, aspect, topographic shading, and time of year with modifications for cloudiness and sunshine hours (Wilson and Gallant 2000). Surface temperature is also extrapolated across the landscape (Sheng, Wilson and Lee 2009). This model is specifically designed for topo- and meso-scale processes so is not ideal for calculation of solar radiation over larger surfaces (Súri and Hofierka 2004).

The r.sun model can be used at various map scales and was developed to overcome shortcomings of other models' limited applicability for larger regions. It is based on the equations published in the European Solar Radiation Atlas (ESRA) and is fully integrated in the GRASS GIS environment (Súri and Hofierka 2004). The r.sun model calculates all three components of solar radiation (beam, diffuse and reflected) for both real sky and clear sky conditions (Súri, Huld and Dunlop 2005). The inputs include elevation, slope, aspect and solar time (Súri and Hofierka 2004). As mentioned previously, one of the main differences between various solar radiation models is the way the diffuse component is handled. The r.sun model is designed to calculate diffuse radiation specifically reflective of European climate conditions (Súri and Hofierka 2004).

2.2.1 Esri's Solar Analyst

Esri's Solar Analyst was developed to draw on the strengths of accurate point specific radiation models while quickly and accurately generating insolation maps over an area of landscape (Helios Environmental Modeling Institute, LLC 2000). It is conveniently available as part of Spatial Analyst extension allowing easy integration with other analysis tools available in Esri's ArcGIS. This model is discussed at length here as it was chosen for use in the work presented in this study.

Solar Analyst calculates solar radiation using the hemispherical viewshed model originally developed by Rich in 1990 and later enhanced by Fu and Rich (1999). A viewshed is the distribution of sky obstruction, or the view of the sky looking upward from each point on the ground (Helios Environmental Modeling Institute, LLC 2000). The model calculates the viewshed for each cell in the input digital elevation model as the visible sky changes based on topography (Fu and Rich 1999).

Solar radiation is presented as global radiation, which is calculated as the sum of direct and diffuse radiation for a point or an area. Direct and diffuse totals are added to determine total global radiation in watt-hours per square meter (Wh/m^2). Reflected radiation is not included in the calculation. The viewshed is overlaid on a direct sunmap to estimate direct radiation and a diffuse skymap to estimate diffuse radiation (Esri 2013a). The sunmap is a representation of position of the sun over time. The sun track for each cell depends on the location and the time of day and year. When calculating direct radiation the tool determines whether the sky is visible or obstructed for each cell in this surface grid, it identifies the solar constant, transmittivity, time duration, the portion of visible sun, and the angle of incidence (Esri 2013a).

Skymaps are used to calculate diffuse solar radiation because it can originate from any sky direction. The entire sky is divided into sectors to create the skymap. Sectors are determined by the zenith and azimuth divisions. The diffuse solar radiation variables identified by the tool for each location include the global normal radiation, the proportion of global radiation that is diffused (this varies between 0.2 for clear sky conditions and 0.7 for cloudy sky conditions), the time interval, the proportion of visible sky, the angle of incidence, and the weighted proportion of diffuse radiation originating in a sky sector

compared to all sectors (Helios Environmental Modeling Institute, LLC 2000; Esri 2013a).

The strengths of this toolset lie in its flexibility. A user is able to account for any time period, site latitude, elevation, surface orientation and atmospheric attenuation (Fu and Rich 1999). The user can set the sky size resolution of the viewshed, the number of azimuth directions used for the viewshed, and the diffuse proportion (based on atmospheric conditions), slope and aspect input types, the amount of azimuth and zenith divisions, and the diffuse model conditions (Esri 2013a).

Despite all its strengths, the Solar Analyst also has limitations in its implementation. As mentioned previously, it does not calculate reflected radiation. Although, Fu and Rich (1999) argue that the contribution from reflected radiation is generally small unless the area has a high albedo. The tool also does not take into consideration cloud cover directly. The user must modify the transmittivity and diffuse proportion to account for these effects. Finally, the tool is only as accurate as the Digital Elevation Model provided as input. In cases where the built environment and surrounding terrain can greatly affect the solar radiation results for the surface, this can be particularly problematic (Fu and Rich 1999).

Generally speaking, with limited snow cover, Hawaii does not have a high albedo on its land surface but cloud cover in the study area can play a significant role in the afternoon. These factors must be taken into account when selecting input parameters. The creation of a high resolution digital surface model (DSM) is also necessary to account for the effects of shading from buildings and vegetation around rooftops.

2.3 Calculating Rooftop Area

This study seeks to calculate the photovoltaic potential for residential rooftops in the town of Kailua Kona. In order to do so, it is necessary to calculate the amount of rooftop space in the study area. As explained by Jakubiec and Reinhart (2012), two of the most crucial components for calculating PV potential include the amount of solar radiation reaching the surface and the amount of useable rooftop area that can be dedicated to photovoltaic panels.

A number of studies have outlined methods to extract building or rooftop shapes for analysis. In many cases the methodologies have relied heavily on the existence of high resolution satellite or remotely sensed imagery. For the most advanced analysis, it is ideal to have 3D models in which individual buildings are represented next to other objects like trees and man-made structures. Nguyen et al. (2012) explain how accurate building generation from Light Detection and Ranging (LiDAR) data requires a number of processes including building detection, object segmentation, roof shape reconstruction, and modeling quality analysis. These techniques are often only possible with high cost data and feature recognition software. In some cases existing building shape or outline datasets are also utilized to assist with building detection and segmentation (Nguyen et al. 2012).

Jo and Otanicar (2011) propose a methodology for quantifying the usable rooftop surface by accounting for existing obstructions like chimneys, air conditioning equipment and skylights that would limit the space available for PV panels. They utilize Quickbird remotely sensed images processed by Definiens Developer software along with existing building shapefiles for the four-square mile study area in Chandler, Arizona (Jo and

Otanicar 2011). The object-oriented analysis utilizes brightness indicators to identify obstructions on rooftops and then calculates shadow effects associated with these objects (Jo and Otanicar 2011).

In situations where advanced processing software and lack of building boundary data are limiting factors, there are other more simplistic techniques employed to estimate available rooftop space. In a pilot study published in Esri's ArcUser magazine, Chaves and Bahill (2010) describe a simple method for isolating building rooftops by classifying suitable elevations as those cells with an elevation greater than or equal to bare earth elevation plus five feet. Similarly, for the Los Angeles County Solar Mapping Portal (2010), ground elevations were first subtracted from the digital surface model and then the Normalized Difference Vegetation Index (NDVI) was utilized to isolate live vegetation within each cell. To create the building surface, live vegetation was removed along cells with a height below eight feet (LA County 2010). Furthermore, a number of authors around the world have explored the relationship between population density and rooftop area. Izquiredo, Rodrigues and Fueyo (2008) use accessible data like population, land use and building density and explore their relationship with roof area in Spain.

Another study of particular interest was completed by Wiginton, Nguyen and Pearce for the province of Ontario, Canada (2010). This study designed a five-step procedure to overcome limited rooftop data. The study area was first stratified based on low, medium, and high population density (Wiginton et al. 2010). A representative sample was then selected from the stratified classes to reflect the distribution of population density within the region. The Feature Analyst extraction tool was then used

to isolate rooftops in the sample set based on available high resolution orthophotos (Wiginton et al. 2010).

Rooftop areas were plotted against population density to determine the existing relationship. Their results indicated a total roof area of 70 m^2/capita +/- 6.2%, although the stratified analysis indicated rooftop area per capita decreases with increasing population density (Wiginton et al. 2010). The equation built from this sample set analysis was used for extrapolation to estimate gross rooftop area for the entire region. The study goes on to reduce overall rooftop area to account for usable area based on characteristics of residential and commercial rooftops in the sample set (Wiginton et al. 2010). Finally, rooftop photovoltaic potential was calculated using the average global insolation and various types of photovoltaic panels (Wiginton et al. 2010).

2.4 Calculating Photovoltaic Potential from Solar Radiation

Understanding available solar radiation and rooftop area are essential components when calculating photovoltaic electricity potential but there are also technological considerations to take into account. These include photovoltaic panel efficacy, tilt, and proper maintenance. Additionally, it is necessary to account for losses during conversion from the photovoltaic produced direct current (DC) to useable alternating current (AC).

In order to assist in understanding the variability associated with PV potential, a number of simulation tools have been created. Some of these specifically complement the solar energy GIS models discussed in the previous section, others use interpolated solar radiation surface datasets. Choi et al. (2011) explain how these efforts have helped overcome existing barriers to implementing PV penetration by providing information needed for design, financing, and operation of PV systems. This section discusses some

of the PV simulation tools available and the variables considered in the formulas utilized to calculate PV potential from solar radiation data.

The National Renewable Energy Laboratory developed the PVWatts (Version 1 and Version 2) simulation tools to estimate energy production for grid-connected crystalline silicon PV systems (Marion et al. 2001). These tools use typical meteorological (TMY and TMY2) solar datasets derived from the National Solar Radiation Database (Marion et al. 2001). PVWATTS Version 1 uses data from 239 existing stations, while PVWATTS Version 2 translates this station data into a 40-km solar radiation grid taking into account global, direct, and diffuse radiation along with monthly temperatures and average surface albedo (Marion et al. 2001; Jakubiec and Reinhart 2012). The user selects the PV system parameters including panel rated size, tilt, orientation and AC to DC derate factor (Marion et al. 2001). The National Renewable Laboratory (2013) suggests a standard derate factor of 0.77 to account for the following system losses: inverter and transformer, mismatch, diodes and connections, DC wiring, AC wiring, soiling and system availability.

Along with their development of the r.sun irradiance calculation model, Súri et al. (2005) also created the Photovoltaic Geographical Information System (PV-GIS) database for Europe and Africa (Choi et al. 2011). The PV-GIS web tool uses the following equation (Equation 1) to calculate the yearly potential of an installed photovoltaic system.

$$\mathbf{E = 365 P_k r_p H_{h,i}} \quad \textbf{Equation 1}$$

Where E is the yearly potential for electricity generation in kilowatt hours (kWh), P_k is the peak power of the equipment installed in kilowatts (kW), r_p is the system

performance ration or derating factor, and $H_{h,i}$ is the monthly or yearly average of daily global radiation in watt-hours (Wh). In the development of the r.sun based PVGIS web calculator, the system performance ratio (r_p) utilized for mono- and polycrystalline silicon panels was .75 (Súri et al. 2005).

Hofierka and Kanuk (2009) also utilize the PVGIS estimation utility for their assessment of photovoltaic potential in urban areas. They suggest a similar formula (Equation 2) where total annual electricity output in kWh for a system is assessed by the following equation:

$$\mathbf{E_{out} = A_e\ E_e\ G} \quad \textbf{Equation 2}$$

Where E_{out} is the annual electricity production in kWh, A_e is the total surface area of solar cells in square meters (m^2), E_e is the annual mean power conversion efficiency coefficient for each PV technology, and G is the annual total global irradiation (Wh/m^2).

This is also quite similar to Clark, Klein and Beckman's formula published in Solar Energy in 1984, where the main variables affecting PV potential include area of the photocells, monthly average hourly radiation, and average efficiency of the array (including any power conditioning equipment).

Beyond module efficiency and standard derating, Jakubiec and Reinhart (2012) suggest derating panel efficiency based on ambient temperature, as temperature is known to have an adverse effect on panel production. In their recent study performed at the Massachusetts Institute of Technology, they incorporated work performed in the National Renewable Laboratory's PVWatts Calculator Version 2 to build the following equations (Equation 3 and Equation 4) to approximate derating of PV panels based on temperature

and point irradiation data at an hourly time step (Marion et al. 2001; Luque and Hegedus 2011; and Jakubiec and Reinhart 2012).

$$\mathbf{T_C = T_{amb} + (T_0 - 20°C)E/800Wm^{-2}} \quad \textbf{Equation 3}$$

Where T_C is the photovoltaic panel temperature °C, T_{amb} is ambient temperature in degrees Celsius (°C), T_0 is the nominal operating cell temperature at ideal conditions °C and E is the incident radiation in W/m^2 at each time step.

$$\mathbf{Pmp = Pmp_0 * [1 + \gamma * (T_C - T_0)]} \quad \textbf{Equation 4}$$

Where Pmp is the derated panel max DC power in watts (W), Pmp_0 is the photovoltaic maximum power at ideal conditions (W) and γ is the temperature correction factor equal to 0.0038 $°C^{-1}$.

Similarly, Choi et al. (2011) also argue that simplistic formulas like that proposed by Hofierka and Kanuk (2009), while easily integrated into GIS software, do not account for intermittent behavior of solar irradiance and the dynamic performance of PV systems. In a study published in Solar Energy, they cite the weaknesses of PV-GIS and PVWatts Version 2 for urban studies as the tools impose a coarse spatial resolution for calculations (Choi et al. 2011). They explain how even though solar modeling tools like r.sun and Solar Analyst allow the user to choose a higher spatial resolution, they are focused on solar irradiation and not the assessment of PV potential (Choi et al. 2011). To combat these weaknesses the authors suggest their PV Analyst extension for ArcGIS which incorporates 4 and 5-parameter PV performance models with irradiance data in TRNSYS (Choi et al. 2011). The PV Analyst extension is intended accurately simulate performances of mono- and polycrystalline silicon PV arrays using data available from

manufacturers including: short circuit current, open circuit voltage, voltage and current at maximum power point, and temperature coefficient of open circuit voltage and short circuit current (Choi et al. 2011).

2.5 Solar Mapping Projects as Decision Support Tools

As mentioned in the introduction chapter, solar mapping applications can be considered GIS-based decision support tools for solar PV potential. These tools assist energy planners, advisors, and policy makers in evaluating the potential for the dissemination of renewable energy technologies. They can also provide a unique benefit by incorporating an analysis of the financial considerations associated with the investment. As stated by Voivontas, Tsiligiridis, and Assimacopoulos, "GIS provides a promising approach that can reveal spatial and time discrepancies of solar potential and energy demand (1998, 419)."

The increased functionality afforded by a mapping application is very useful for the potential solar adopter. Common mapping applications for solar potential allow the user to identify their location and specific household characteristics to get a series of predictions of production from PV system, electricity savings in dollars, carbon savings, system payback, and information on local incentive programs (Jakubiec and Reinhart 2012). Jakubiec and Reinhart (2012) explain how these websites rely on various GIS modeling techniques that differ based on solar radiation calculations, spatial and temporal accuracy of data, and software used to perform the analysis.

For the most part, a handful of GIS-based solar radiation models have been employed to generate the majority of solar maps created for U.S. municipalities. For the eleven solar potential maps created for popular North American cities reviewed by

Jakubiec and Reinhart (2012), the most commonly used methodologies for rooftop irradiation maps include the National Renewable Energy Laboratory PVWatts calculator and Esri's Solar Analyst.

While an abundance of literature about city and municipal solar mapping projects exists, there is rather limited information available on similar efforts in rural communities. Lietelt (2008) explains how the lack of integration of solar mapping into communities less dense than larger cities and municipalities may be attributed to limited interest or the unavailability of suitable data. This research initiative seeks to identify and implement suitable techniques for mapping solar PV potential on the Island of Hawaii, a County with a low population density of about 45 people per square mile.

2.6 Hawaii Solar Mapping Projects

To date, a handful of solar modeling and mapping efforts have been undertaken in the State of Hawaii. They are described in the remainder of this chapter. The main contributors to this work have been the United States Department of Energy through the National Renewable Energy Laboratory (NREL), the Hawaii Natural Energy Institute (HNEI) at the University of Hawaii at Manoa, the State of Hawaii Office of Planning and Department of Business, Economic Development and Tourism, and the utilities including the Kauai Island Utility Cooperative (KIUC) and Hawaii Electric Company (HECO) and its subsidiaries. The various efforts are described below by Island.

2.6.1 Oahu

In 2012, HNEI jointly sponsored a solar modeling and integration study with NREL and HECO, which was presented at the 2nd Annual International Workshop on Integration of Solar Power in Power Systems Conference (Piwko et al. 2012). This study

focused on the Island of Oahu and was a follow up to the Oahu Wind Integration Study completed in 2010 (Piwko et al. 2012). This solar integration study looked at the impact of higher penetration of solar energy into the Oahu electric grid from both centralized and distributed PV plant scenarios (Piwko et al. 2012).

The solar data developed for this work consisted of 2-second solar power production profiles for Oahu and downward shortwave radiation every ten minutes during 2007-08, for every point on a one kilometer spaced grid over all the Hawaiian Islands (Matthias Fripp, Professor University of Hawaii, email 28 March 2013). These datasets were developed with the AWS Truepower proprietary software using weather station data from 2007-2008 (Piwko et al. 2012; AWS Truepower 2013). The software utilizes a Numerical Weather Prediction (NWP) model coupled with a stochastic-kinematic cloud model (Piwko et al. 2012). This data had not been published for use in the public domain at the time of this research project was underway.

The Blue Planet Foundation, a local nonprofit organization committed to Hawaii's clean energy future, has developed a Solar Portal that is currently in beta testing (blueplanetfoundation.org/solar-portal.html). The portal is designed to be a resource for both existing and new solar installation customers providing location information and resources including contractor information and educational videos. The site does not incorporate incoming solar radiation information but rather provides the location of existing solar PV and solar thermal hot water systems allowing users to search their neighborhood and add comments and feedback about their solar systems and contractors. At the time this research was conducted the main sources of data for the portal were the

City and County of Honolulu and the Department of Planning and Permitting. Installation locations were listed only for Oahu, neighbor-island data was still pending.

The State of Hawaii has also recently added a solar roof potential 3D model with coverage from downtown Honolulu to Diamond Head (State of Hawaii Office of Planning 2013). It is available for download at the Office of Planning, Statewide GIS Program website. This data was produced by CyberCity 3D, and acquired by the Hawaii State Office of Information Management and Technology in February 2013. The data was derived from 2008 remote sensing imagery and converted to 3D models using CyberCity proprietary software (State of Hawaii Office of Planning 2013). This data includes building rooftop height and area along with their solar potential. CyberCity 3D quantifies solar potential assessing the roof angle, surface area and solar azimuth (orientation). This dataset characterizes solar potential based on a ranking of 0- no to low solar potential, 1- medium solar potential, and 2- high solar potential. Roof areas with a high solar potential (2) are those with a minimum of 100 square feet and an orientation from 161 degrees to 200 degrees (State of Hawaii Office of Planning 2013).

2.6.2 Kauai

The National Renewable Energy Laboratory in conjunction with Kauai Island Utility Cooperative, has conducted an island wide solar photovoltaic assessment in Kauai (Helm and Burman 2010). This project customized the In My Back Yard (IMBY) software that utilizes the PVWatts performance model to Kauai environmental conditions and utility load information. The goal of the project was to create created a tool help promote renewable adoption on the Island (Helm and Burman 2010).

Appropriate commercial rooftop area was estimated using satellite imagery and taking into account aspect, rooftop obstructions and shading potential. Rooftops were chosen mainly because of their large area unobstructed by air conditioning equipment. The findings identified 136,412 square meters of useable commercial rooftop area for photovoltaic installations and calculated a total potential of 15,938 MWh/year (Helm and Burman 2010). The study did not, however, address the economic feasibility of installing PV on the suggested areas.

2.6.3 Hawaii Island

The Hawaii Natural Energy Institute (HNEI), in conjunction with Hawaii Electric Light Company, currently has a project examining the performance of PV arrays within the different microclimates of Hawaii Island (Hawaii Natural Energy Institute 2012). Solar radiation and weather data is collected at one-second intervals and stored within the HNEI database (Larry Cutshaw, HNEI Project Manager, phone conversation 28 December 2012). The goal of this project is to better interpret the interconnection between weather conditions and PV performance. This data is currently being analyzed and no report has been publicly released at this time.

2.6.4 Statewide

The Office of Planning, Statewide GIS Program website houses two solar spatial datasets for public use. The first is a monthly and annual solar resource potential 10-kilometer grid measured in global horizontal irradiance and direct normal irradiance. This GIS data was developed by NREL using the Perez model from the State University of New York/Albany (NREL 2013). It is worth noting that with a spatial resolution of 10 kilometers there is little confidence in the accuracy of this dataset. The metadata

associated with this dataset states that modeled values are only accurate to approximately 15 percent of a true measured value in the grid (State of Hawaii Office of Planning 2013). This is attributed to the terrain effects and microclimate influences including local cloud cover that can vary significantly over short distances (State of Hawaii Office of Planning 2013).

The second, and perhaps the most commonly utilized solar dataset, is the solar radiation polyline dataset commonly referred to as the "Solar Zone Map." These polylines were digitized from 1985 Sunshine Maps of varying scales (State of Hawaii Office of Planning 2013). The data displays solar zones measured in calories/cm^2/day. Solar zones range from 200-650 calories/cm^2/day. These zones were compiled based on old Hawaii Sugar Planters Association anemometer solar data (State of Hawaii Office of Planning 2013). This dataset is also served on the Department of Business Economic Development and Tourism web map "EnerGIS" (DBEDT 2013b).

With only two low-resolution solar datasets currently available for Hawaii Island, there are limited mapping resources to help commercial and residential facilities identify their own solar potential. The literature and mapping applications reviewed here were used to inform the development of the methods for this study. The methodology described in the following section seeks to incorporate higher resolution data and GIS solar modeling tools to better quantify total photovoltaic potential for residential rooftops.

CHAPTER 3: METHODS

This chapter begins with further elaboration on the study area characteristics and a description of the data utilized in this research. The research design is then presented and methods for determining the rooftop sample set, calculating incoming solar radiation and analyzing rooftop points are discussed in detail. The final section presents the methods for performing statistical analysis to generate the equations needed for extrapolation to estimate total PV potential for the study area.

3.1 Description of Study Area

The town of Kailua Kona, on the leeward side of the Big Island was chosen for this study (Figure 3.1). The Big Island is centered at 19.63 N, 155.52 W and measures 8,150 Km^2. The island is often described as a warm tropical environment but, in fact, climate on the island varies greatly over relatively short distances. The average temperatures on both the leeward and windward side of the island range between average highs from 75 to 83 F° with average lows between 57-70 F° (Western Region Climate Center 2012). The large volcanic mountains of Mauna Loa and Mauna Kea dominate the island physiography. This mountainous terrain is the largest influence on climate variability with windward coasts receiving over 130 inches of rain annually while the leeward coasts see less than 30 inches of precipitation (Western Pacific Regional Fishery Management Council 2012). Calculation of solar radiation and PV potential on the Big Island presents a unique set of challenges with the highly variable weather conditions and elevations creating multiple microclimates. The study area was selected to ensure the highest resolution data were used to assess solar radiation (Figure 3.1). The boundaries were defined by the availability of LiDAR data.

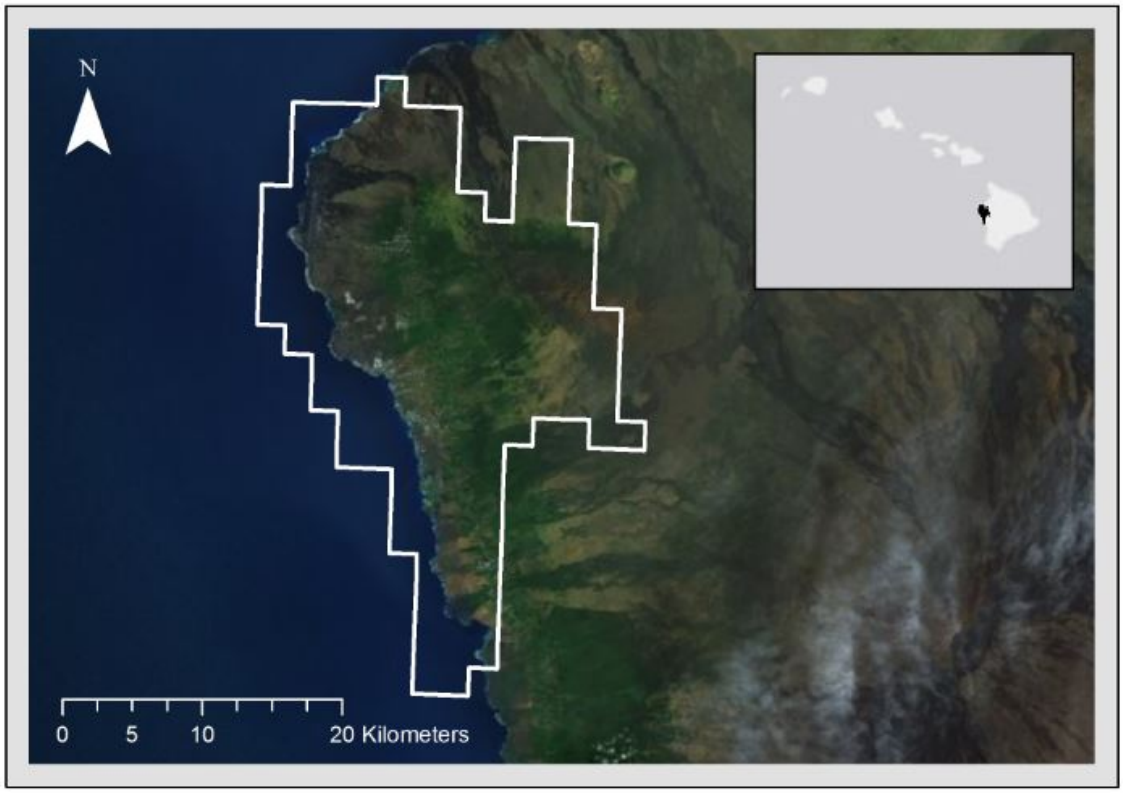

Figure 3.1 Study area LiDAR coverage

3.2 Data

3.2.1 LiDAR data

Light Detection and Ranging (LiDAR) data was utilized for the creation of the digital surface model (DSM). Point-cloud files were obtained from the Hawaii State Office of Planning, Statewide GIS Program. Data was originally collected on July 14, 2006 by Airborne1. Data was obtained in ASCII raw format in UTM Zone 5.

Point cloud data is a type of vector data in which spatial location is explicitly stored in each point (Chen 2007). A high density point cloud therefore has a much larger file size than imagery with the same resolution (Chen 2007). In order to allow for easier management of the files, the raw point files available for the study area were separated into 156 tiles.

The ASCII data obtained for this study included XYZI point files for all points, ground points, and extracted points. This means that all points were filtered into ground and non-ground returns to create the ground points and extracted points. For this study, the extracted points were selected to create the digital surface model (DSM). The extracted points contain the height information for the built environment and vegetation on the ground. The bare earth, or ground points, have been removed.

The workflow for creating the DSM from the available LiDAR ASCII data was adapted from the workflow presented by the County of Los Angeles-Solar Mapping Portal (LA County 2010). Using tools in the ArcMap 3D Analyst extension, the raw LiDAR extracted point files were processed into terrain rasters that served as the digital surface models for input into the solar radiation analysis.

The Esri point file information tool was used to generate a summary of the characteristics for each tile including the number of points, average point spacing, z min, and z max. The raw extracted point data files were processed to multipoint feature classes. The new feature classes were then added to a feature dataset. Terrain datasets were generated within these feature datasets. Average point spacing was determined from the point file information tool findings for each tile. The Terrain to Raster tool was used to produce a rasterized surface model model. This step created the surface grid from the terrain. Cell size was set to 2 meters after consideration of the average point spacing for each tile. An example of the final product is displayed in Figure 3.2. This graphic illustrates the surface of the land including buildings and vegetation heights.

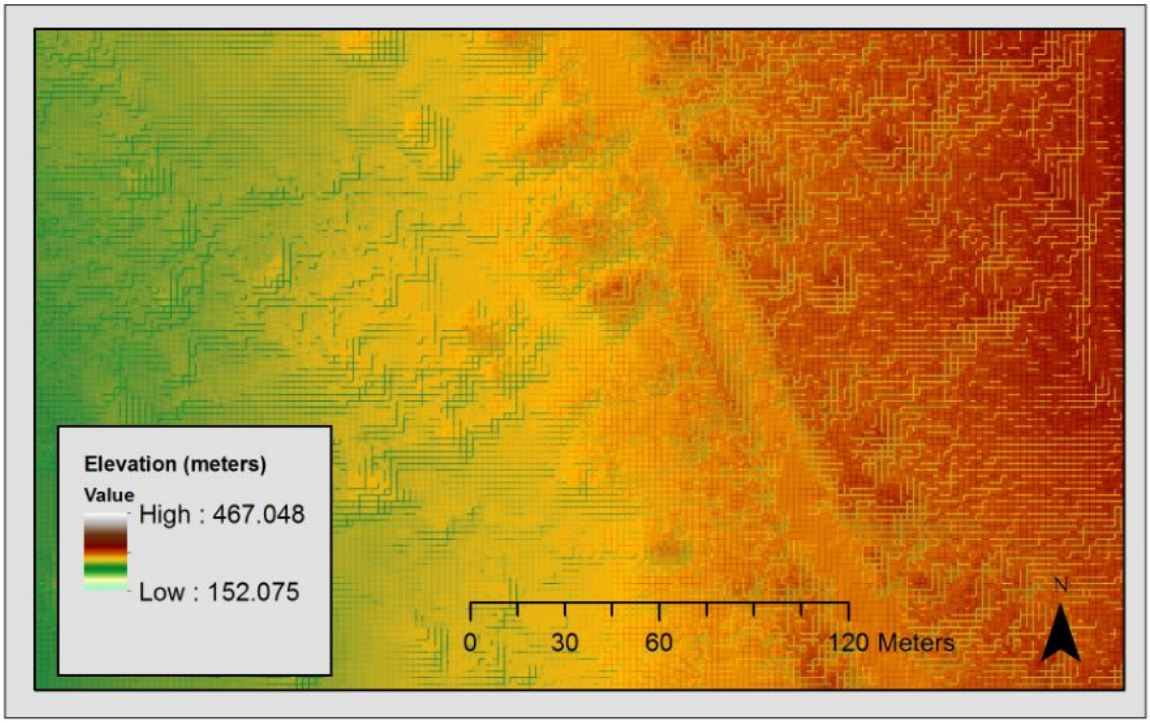

Figure 3.2 Elevation with 2-meter spatial resolution from LiDAR

3.2.2 Tax Map Key Parcel Data

The tax map key (TMK) parcel data is a polygon shapefile that was also obtained from the Statewide GIS Program (State of Hawaii Office of Planning 2013). The TMK parcel data was originally in UTM Zone 4, North American Datum (NAD83), but was projected into UTM Zone 5 for proper alignment with the Hawaii digital surface data. The dataset was created by a local agency, Geographic Decision Systems International, and is maintained by Hawaii County. The last update was July 2011.

The TMK parcel data played an integral part in this research design. This is the most comprehensive list of parcel characteristics available to the public containing a number of attributes for each lot. The most relevant to this study are displayed in Table 3.1. The TMK number is the unique identifier for each parcel. The parcel index (PITT) code is the tax category applied to the property and the Homeowner attribute designates

the existence of a home. Attributes were sorted by PITT code to identify the residential parcels and then unoccupied lots were eliminated by filtering for the Homeowner attribute. This process identified the pool of residential lots to be considered for analysis of PV potential.

It is important to note that the parcel data does not have any building square footage data recorded. Without any existing rooftop or building structure size data for the study area, the parcel area (lot size) was used to analyze against a digitized rooftop sample to look for correlations.

Table 3.1 Tax map key (TMK) parcel data attributes

Attribute	Description
TMK	Unique 9 Digit Tax Map Key Number
PITT code	Used to identify tax rate applied to the property (examples include residential, commercial, and industrial)
Homeowner	Homeowner on property (Yes, No, Unknown)
Shape Area	Lot Size

Source: State of Hawaii Office of Planning, State GIS Program 2013

3.2.3 Aerial Imagery

The Bing Maps Aerial Imagery was used as the reference for digitizing rooftops from building outlines. It offers worldwide orthographic aerial and satellite imagery with the most detailed coverage in the United States and the United Kingdom (Esri 2013b). Bing Maps was chosen as the basemap over the ArcGIS online World Imagery Map Service as it displayed at a higher resolution with less cloud cover over study area parcels.

3.2.4 PV Production on Active Residential Site

Real time PV production data was provided by a local resident. This data was used for a comparison with PV potential modeled in this study. The performance of this

residential 2 kilowatt, 12 inverter photovoltaic system is logged through the EnPhase Energy Products website (enlighten.enphaseenergy.com). The dashboard allows the user to see search the installation by location. The system size, lifetime production and number of microinverters are displayed. It also documents the daily, monthly, and annual performance of each panel installed. Historical output reports can be generated based on user defined time periods. This interface was used to generate total production reports for 2012 and January – June 2013 for the location.

3.3 Research Design

Once the available data sources were identified a number of tasks were outlined in order to estimate total rooftop photovoltaic potential for the study area. It was first necessary to identify a sample of parcels for which to digitize rooftops. These sample rooftops and the rooftop with real time PV production were digitized. The terrain parameters and solar radiation were then calculated for those rooftops. These rasters were converted to vector points to perform a spatial join with rooftops. The average slope, elevation, and solar radiation were spatially joined to each rooftop so that PV potential could be calculated. The variables for each rooftop were used for statistical analysis of the relationship between rooftop and lot size, as well as multiple linear regression for average and total rooftop PV potential. Finally, the equations built were applied to the entire study area. Figure 3.3 outlines the research design and the remainder of the chapter discusses each step in detail.

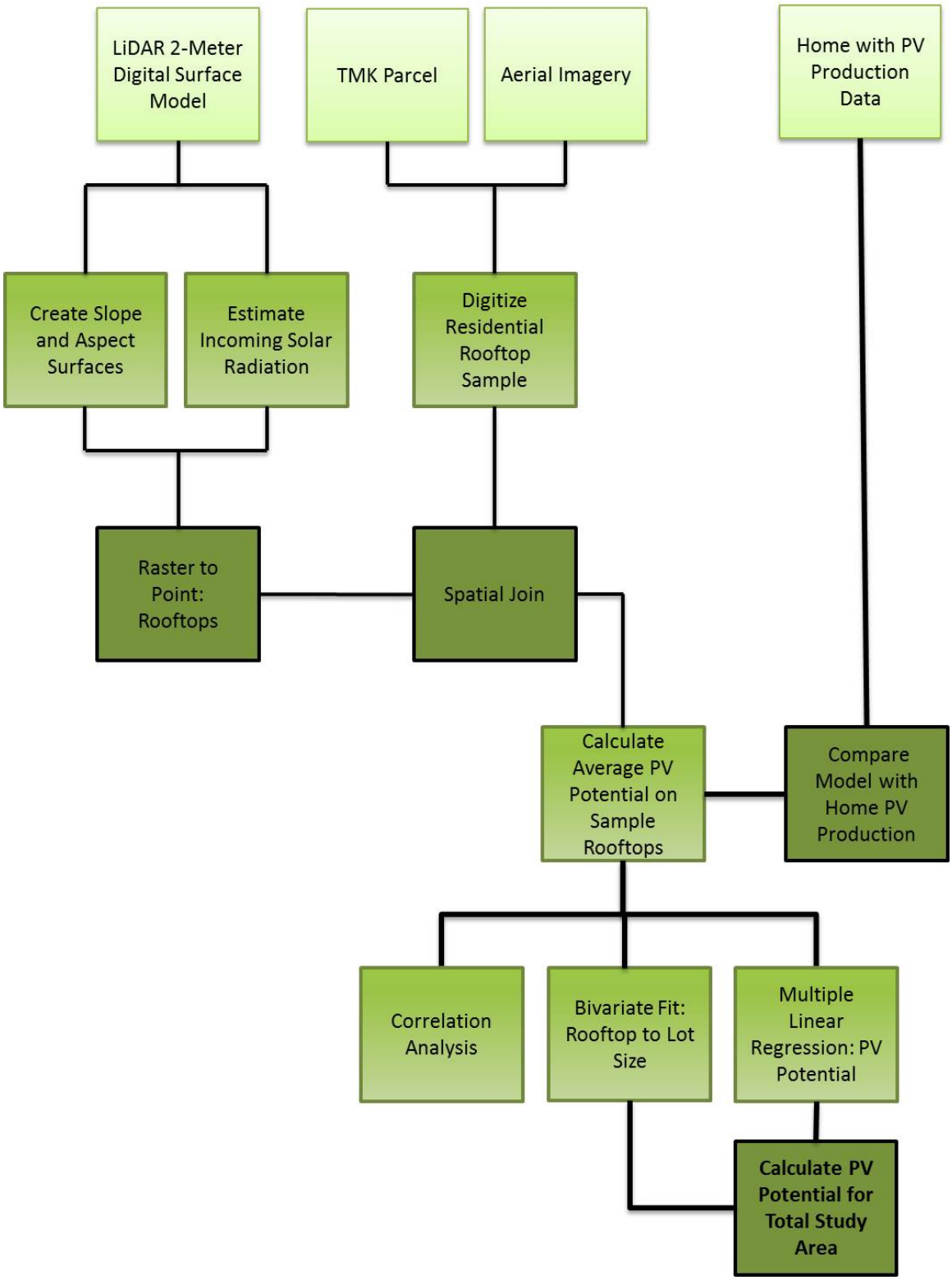

Figure 3.3 Flowchart for calculating PV potential for this study

3.3.1 Isolating Building Rooftops for Sample Set

The rooftop isolation methods discussed in the literature review chapter refer to methods for mapping urban environments using LiDAR, 3D modeling and other higher resolution data sources (Jo and Otanicar 2011; Nguyen et al. 2012). In these cases, the rooftop area calculation for each location is a part of an automated process. For this study area, automated rooftop estimation was not possible as there were no existing building footprint shapefiles available. It was also not possible to isolate existing tree vegetation from building structures when processing the LiDAR point files into the digital surface model. Without the option to automate building extraction, the sample set of rooftops needed to be hand digitized for analysis. Due to time constraints, it was not feasible to analyze every rooftop in the study area so the decision was made to follow similar methods as those proposed by Wiginton et al. 2010 and use a sample set of rooftops to characterize the region. This was accomplished in the two steps described below.

3.3.1.1 Stratified Parcel Selection

A representative sample of rooftops was selected by analyzing the available parcel dataset. The hypothesis was that available parcel area (lot size) data would display a correlation with the rooftop size and this relationship could be used to extrapolate out to the entire study area.

The sample rooftops to digitize were chosen using stratified random parcel selection based on the TMK parcel area found in the attribute table. There were a total of 15,676 parcels in the study area. The study area was comprised of parcels of all tax classifications (PITT Codes Table 3.1) including residential, commercial, apartment, industrial, agricultural and rural, conservation, hotel and resort, unimproved residential

and homeowner. Parcels were first sorted for residential tax codes then filtered to identify those with a homeowner classification. This resulted in 4,694 parcels with single family dwellings located on them.

The size distribution for the 4,694 parcels was then analyzed using JMP software. Outliers with areas in the smallest 0-2.5 percent and largest 97.5-100 percent were removed. The result was 4,460 eligible study area parcels. The parcel area stratified classes are displayed in Table 3.2. There are six classes based on lot size. Table 3.2 displays the number of parcels that fall within each class and the size range of the lots.

Classes were created to ensure the sample chosen for digitizing was representative of the range of lot sizes in the study area. This was done strategically for future analysis of the correlation between lot size and rooftop size.

Table 3.2 Stratified parcel selection

Class	Percentage	Total Parcels	Lot Size Range (m^2)
1	2.5-10%	352	536 – 688
2	10-25%	704	688 – 766
3	25-50%	1,174	766 – 958
4	50-75%	1,174	958 – 1,419
5	75-90%	704	1,419 – 1,893
6	90-97.5%	352	1,893 – 3,026

In order to create an appropriate sample size, the Creative Research Systems (2012) sample size calculator was utilized. It was determined that a population of 4,460 parcels a 5 percent sample size (or 223 parcels) results in a 95 percent confidence level and confidence interval of 6.4. Table 3.3 displays the breakdown of the number of samples to digitize for the 5 percent sample size for each class. The resulting 223 parcels for digitizing were chosen at random using Microsoft Excel.

Table 3.3 Sample design for digitization

Class	Total Parcels	Samples to Digitize
1	352	17
2	704	36
3	1,174	59
4	1,174	58
5	704	36
6	352	17
Total	4,460	223

3.3.1.2 Digitizing Rooftops

The built in Bing Maps Aerial Imagery was chosen as the base map to digitize for reasons discussed in Section 3.2.3. The rooftop feature class was digitized at the highest resolution possible given (between 1:500 to 1:1,000). An example of digitized rooftops is displayed in Figure 3.4.

Figure 3.4 Sample set of rooftops

3.3.2 Estimating Terrain Parameters and Incoming Solar Radiation

The sample set rooftops were used to determine the LiDAR tiles needed for analysis of terrain parameters and solar radiation. For each tile where sample set homes were located, the slope, aspect and solar radiation was also calculated.

3.3.2.1 Terrain Parameters: Slope and Aspect

The 2-meter LiDAR elevation data provided the raster surface input to run the slope and aspect tools in the ArcGIS toolbox. This resulted in an output aspect raster and an output slope raster. The aspect, or orientation, was calculated in degrees measured clockwise from north 0 - 359.9°. The inclination of slope was also calculated in degrees, from 0 - 90°. Examples of the aspect and slope are displayed in Figure 3.5 and 3.6. These figures display a small section of the study area with three sample rooftops.

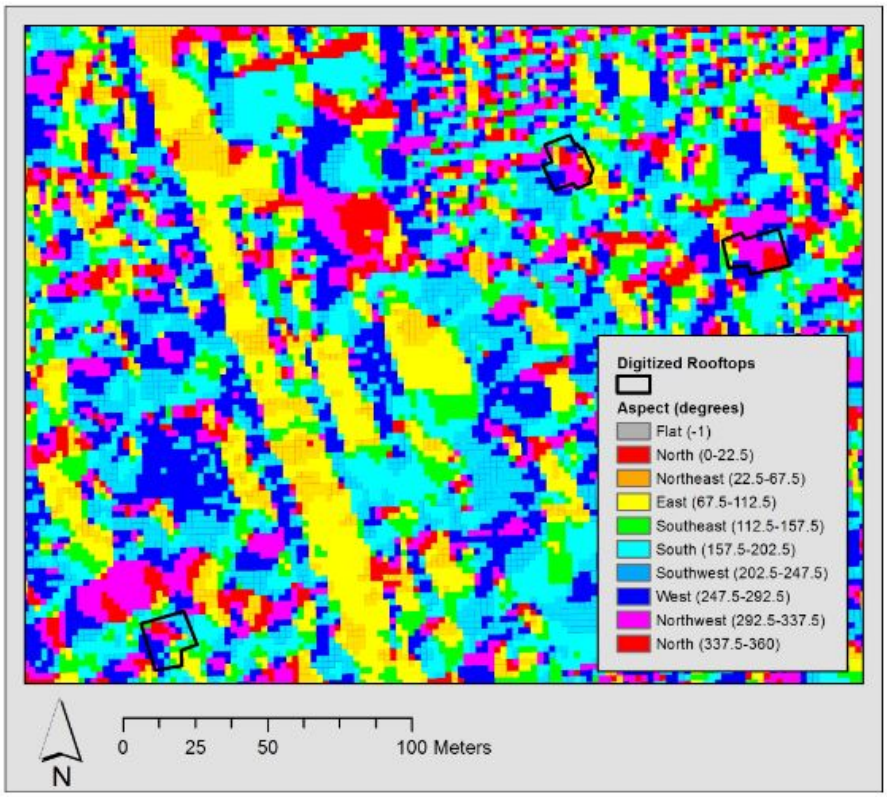

Figure 3.5 Map showing aspect

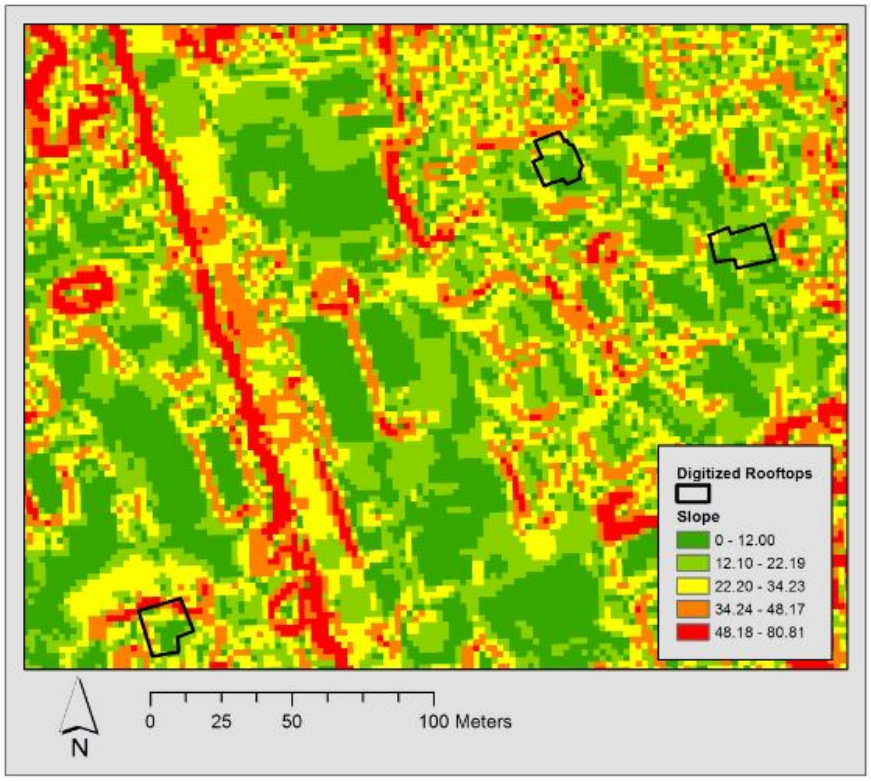

Figure 3.6 Map showing slope

3.3.2.2 Estimating Solar Radiation

Using GIS to model solar radiation provides a convenient way to generate insolation maps and relate them to other spatial data (Fu and Rich 1999). The Esri toolset was chosen as the appropriate GIS modeling tool for calculating solar radiation for this project.

The main input for the tool is a digital elevation model (DEM) or digital surface model (DSM). In this case, the 2-meter resolution LiDAR provides the latitude for the site area, the slope and the aspect for each cell. The user determines a number of conditions for the remaining tool parameters. Table 3.4 displays the input parameters were selected to create the solar radiation surface for this study.

The sky size sets the resolution of the viewshed, sky map and sun map; which determines the number of calculations that take place to estimate the direct radiation reaching each cell in the surface grid. The default is 200 x 200 cells but increasing sky size increases accuracy. Multiple trials were run to balance calculation time with desired accuracy of results. Unfortunately, processing time increased greatly with higher resolution values of 400 x 400 and above. Upon further research it was determined that, when testing their model performance Fu and Rich (1999) found highly similar results from both 200 x 200 and 400 x 400 viewshed resolutions, so the decision was made to utilize the default values for this input parameter. The calculation direction input sets how many directions are used when calculating the viewshed. Thirty-two (32) is the default and is considered sufficient for complex mountain topography (Fu and Rich 1999). The azimuth and zenith divisions relate to how many divisions are used to create the sky map. The default, 8, was selected for each.

The time period for which the insolation is calculated can be set to within one day, multiple days, specific days or across the whole year (Esri 2013a). For this case, the maximum range of one year was chosen. The user must then choose the day interval and hour interval. These variables also relate to sky size. When the sky resolution is set to the default it is important to have a day interval greater than 14. In this case where time configuration is set to one year, the day interval is disabled by the tool in order to calculate on monthly calendar intervals (Esri 2013a). The hour interval indicates the time used for calculating sky sectors of sun maps. The default of 0.5 hour was chosen.

Finally, the user must indicate the parameters having to do with how diffuse radiation is calculated. Standard overcast sky was chosen for the diffuse model type. This

Table 3.4: Input parameters for area solar radiation tool in ArcGIS

Input	Description	Value
DEM	Input elevation parameters from surface raster layers.	2 meter-LiDAR
Latitude	Latitude of site area, units are in decimal degrees.	19.5º N (Automatic input from raster)
Sky Size	Resolution of the viewshed, sky map and sun map, upward looking representation of the sky.	200
Time Configuration	Specifies the time configuration period used for calculating solar radiation: within a day, multiple days, special days, or whole year.	Whole year 2013
Day Interval	Time interval through the year (units: days) used for the calculation of sky sectors for the sun map.	(monthly)
Hour Interval	Time interval through the year (units: hours) used for the calculation of sky sectors for the sun map.	.5
Each Interval	Specifies whether to calculate a single total insolation value for all locations or multiple values for the specified hour and day interval	No interval
Z Units	Number of ground x,y units in one surface z unit.	1
Slope Aspect Input Type	How slope and aspect information are derived (either from DEM or Flat surface).	From DEM
Calculations Directions	Number of azimuth directions used when calculating the viewshed (multiples of 8, 32 is default).	32
Zenith Divisions	Number of divisions used to create sky sectors in the sky map, default is 8 divisions relative to zenith.	8
Azimuth Divisions	Number of divisions used to create sky sectors in the sky map, default is 8 divisions relative to north.	8
Diffuse Model Type	Type of diffuse model- uniform sky, the incoming diffuse radiation is same from all directions OR standard overcast sky- standard overcast diffuse model varies with zenith angle.	Standard overcast sky
Diffuse Proportion	The proportion of global normal radiation flux that is diffuse (0-1).	0.3
Transmittivity	Relates to cloud cover, fraction of radiation that passes through the atmosphere averaged over all wavelengths, values range from 0-1, 0 is no transmission and 1 is all transmission, .5 for a generally clear sky.	0.5

Source: Descriptions from Esri 2013a Desktop Help

ensures incoming diffuse radiation is calculated for each zenith angle (Esri 2013a). The diffuse proportion and transmittivity have an inverse relationship. The diffuse proportion indicates the amount of global normal radiation is that is diffuse and the transmittivity indicates the amount of radiation that passes through atmosphere. The defaults were chosen, 0.3 and 0.5 respectively (Esri 2013a).

Figure 3.7 displays an example of the final annual solar radiation calculated for 2013, for the same part of the study area displayed in the slope and aspect figures. Incoming solar radiation in this example displays a minimum of 123.6 kWh/m^2/yr and maximum of 1,767 kWh/m^2/yr.

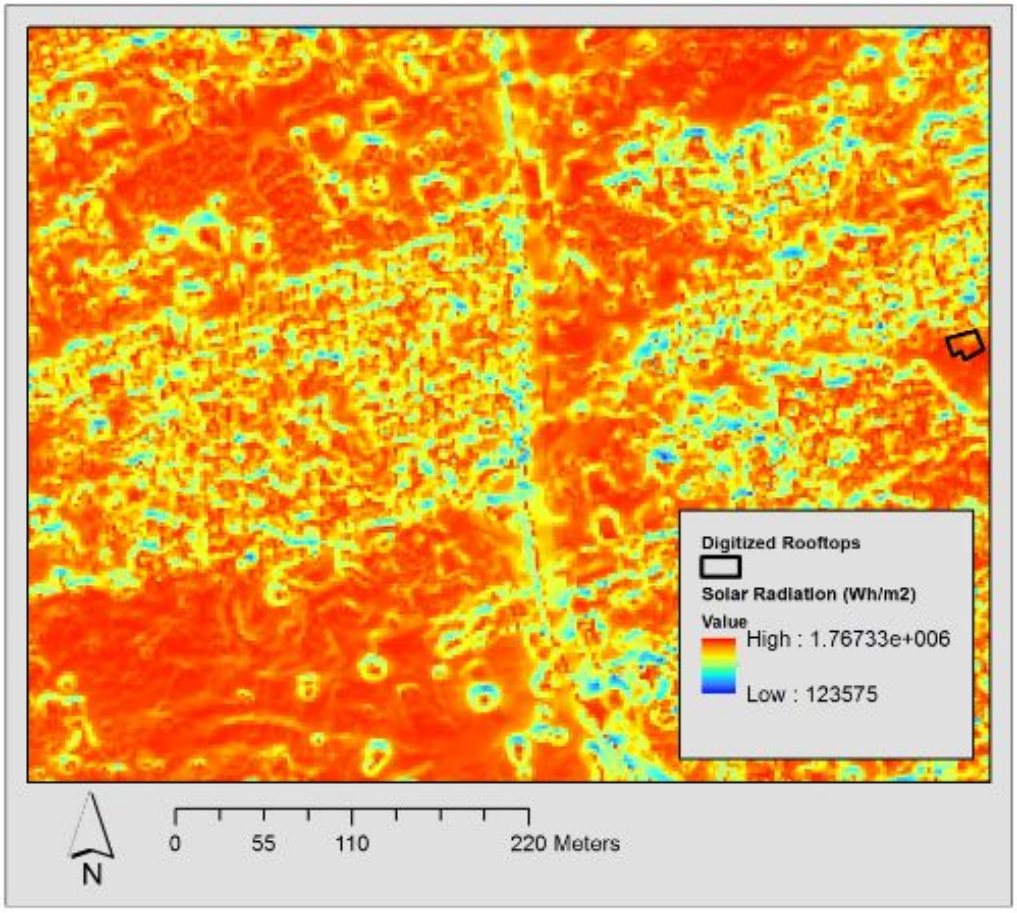

Figure 3.7 Incoming solar radiation surface

3.3.3 Spatial Analysis for Selected Rooftops

Once the sample rooftops were identified and the elevation, slope, aspect and solar radiation were generated for the area, it was necessary to compile the findings so that PV potential on each rooftop could be calculated.

3.3.3.1 Raster to Point

The elevation, slope, aspect and solar radiation rasters were converted to vector point layers in order to prepare for spatial analysis with the rooftop polygon layer. Using the Raster to Point tool in the toolbox, each cell was converted to a point in an output feature class. Each elevation, slope, aspect and solar radiation cell value became an attribute in the point layer feature classes.

Using the Clip tool, the rooftop polygon feature class was used to isolate the terrain and solar radiation points falling specifically on the buildings and eliminate the remaining areas from the point feature classes (Lietelt 2010). An example of the solar radiation points within rooftops is displayed in Figure 3.8.

Figure 3.8 displays a significant variation in the range of solar insolation (340-1,750 kWh/m^2/yr) reaching the sample rooftops pictured. The higher solar radiation areas appear to be located on the southeast corners of both rooftops but there are some high insolation points scattered on the northern edge of each rooftop as well. Variance in rooftop insolation is not uncommon and can be attributed to a number of causes including building structure orientation, shading from surrounding vegetation, and drastic elevation changes. It is not, however, clear from the findings displayed in Figure 3.8 whether any of these variables are influencing factors that would cause these divergent results. This warrants further investigation into the characteristics of the area in order to assess the

quality of the solar rooftop points. To do so, the solar radiation points (Figure 3.8) and aspect points (Figure 3.9) were compared to a high resolution image of the location obtained from Google Earth (Figure 3.10).

Figure 3.8 Points of solar radiation on rooftop

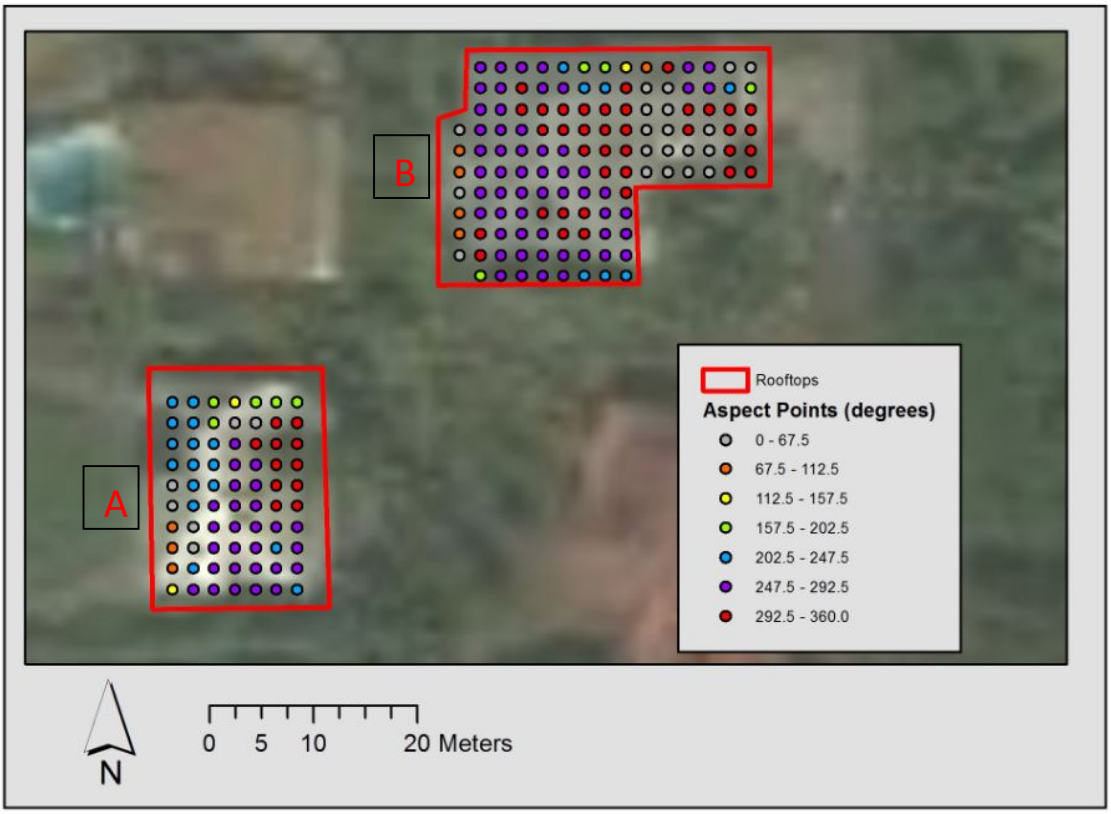

Figure 3.9 Aspect points on rooftop

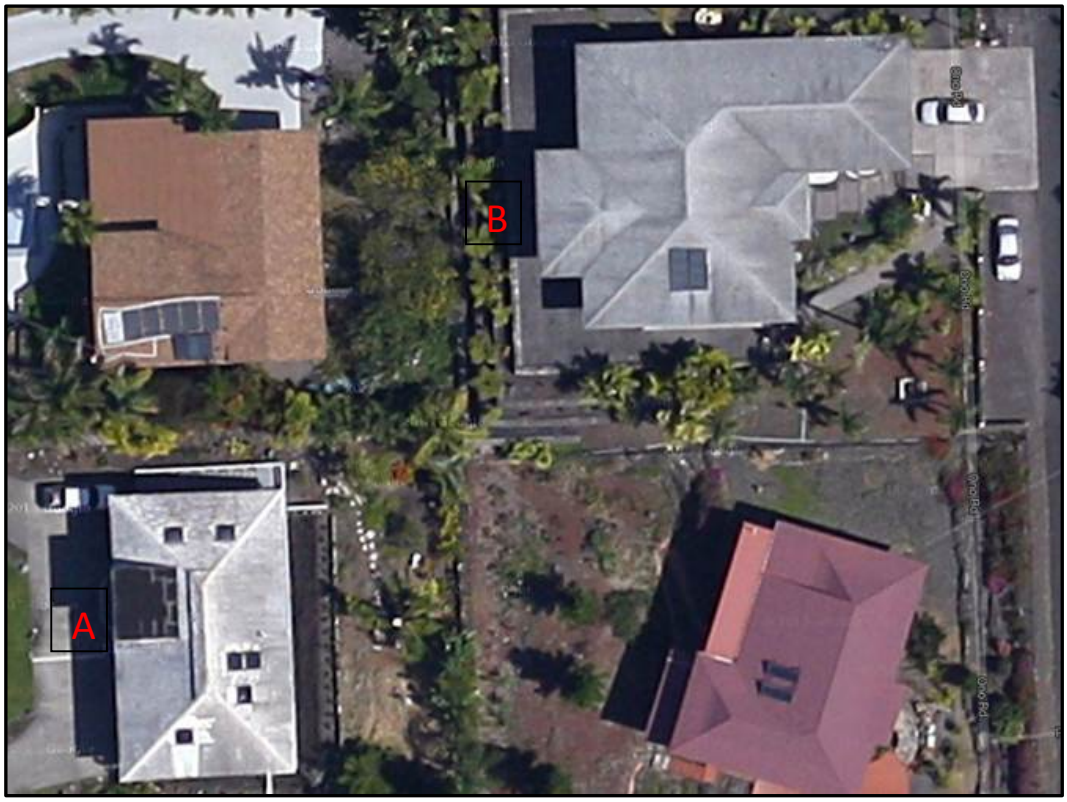

Figure 3.10 High resolution sample rooftop image from Google Earth

The use of the Google Earth image allowed the critical evaluation of the reliability of the rooftop point data. Overall, the comparison of all three figures highlights some inconsistencies that cause concern over the quality of the rooftop point solar radiation data. Both properties have tree landscape around their perimeters but there are no large tree stands or continuous vegetation areas that would significantly shade the portions of the rooftops from incoming sunshine. Moreover, the aspect points (Figure 3.9) do not appear to correspond with the actual orientations of the rooftop surfaces (Figure 3.10). In Figure 3.10 the upper right hand sample rooftop (B) displays a complex rooftop with varying roof levels and directions. The lower left hand rooftop (A) seems to have four main orientations with some smaller skylights or objects located on the surface. In Figure 3.9, the majority of aspect points on both rooftops are west facing. The other orientations, while less represented, are scattered and do not seem to align with the symmetrical rooftop divisions displayed in Figure 3.10.

3.3.3.2 Spatial Join

While the solar insolation point data was initially considered the ideal representation for calculating PV potential from incoming solar radiation, the lack of consistency between Figure 3.8 and 3.9 and the available imagery and led to an approach considering average incoming solar radiation on rooftops. The spatial join tool was used to create a final feature class layer containing the average elevation, slope, and solar radiation for each rooftop. This tool joins the attributes from one feature (the join feature class) to another (the target feature class) based on their spatial relationships (Esri 2013c). Each point layer was set as the join features to the rooftop target feature class. The Join operation was set to JOIN_ONE_TO_ONE with the merge rule specified as Average.

Therefore the output layer contained the 224 rooftops (223 samples and one rooftop with real PV production) with the average elevation, slope and incoming solar radiation. The attributes of the final rooftop layer are outlined in Table 3.5. The aspect point layer was not joined to the rooftop layer as it was not possible to average the directional degrees and get an accurate representation of orientation.

Once the elevation, slope and solar radiation points were spatially joined to the rooftop polygon layer, the final layer was exported to Microsoft Excel for statistical analysis of the variables and their relationship to photovoltaic potential.

Table 3.5: Final rooftop layer attribute table used for PV potential calculation

Column	Unit	Description
OBJECT ID	Numeric	Unique ID for each rooftop
Join Count	Numeric	Total number of data points within shape area
TMK Number	Numeric	Tax map key number for parcel where rooftop is located
Average Elevation	Meters	Average of elevation points within shape area (output of LiDAR elevation surface)
Average Slope	Degrees	Average of slope points within shape area (Output from slope raster)
Average Incoming Solar Radiation	Watt-hours per square meter per year ($Wh/m^2/yr$)	Output from Area Solar radiation tool; average of incoming solar radiation points within shape area
Rooftop Area	M^2	Area of digitized rooftop
Parcel Area	M^2	Area of parcel where rooftop is located
Parcel Class	Number	Class used for stratified parcel selection

3.3.4 Calculating PV Potential on Building Rooftops

Although solar radiation is one of the largest factors in calculating photovoltaic generation potential, other factors like technology, orientation and maintenance play important roles as well. As discussed in the literature review, many web-based GIS solar tools use simplified formulas to assess PV potential. In most cases, calculating the PV potential requires a consideration of different output capacities the type of the panels or system in place. Súri et al. (2005) suggest Equation 1 presented in the literature review for estimating PV potential. This equation was chosen for this evaluation as it incorporates both the peak power rating for the panel type and a system performance ratio.

The peak power rating is a reflection of the efficiency of the PV technology under consideration. Each available model has a specific peak power rating under standard test conditions (STC) and PVUSA test conditions (PTC). Standard test conditions reference model output at 1000 W/m^2 solar irradiance and 25^oC PV module temperature (NREL 2012). PVUSA test conditions are designed to be a better reflection of real world conditions.

Neither STC nor PTC ratings account for system losses from converting from direct current to alternating current. Variables like wiring, transformers, or inverters all affect panel output. This is typically accounted for by a derating factor, which can also be referred to as the conversion coefficient or performance ratio. As mentioned in the literature review, Súri et al (2005) suggest a typical performance ratio for mono- or polycrystalline silicon panels of 0.75. Hofierka and Kanuk (2009) use a default value of 0.766 for the power conversion efficiency coefficient for crystalline silicon. For this

study, a performance or derate factor of 0.77 was chosen as this is the standard utilized by NREL (2013) PVWATTS and commonly accepted by industry professionals in Hawaii.

On Hawaii Island, one of the most common photovoltaic panels installed is the SolarWorld SW260 monocrystalline panel (Jim Garber, Inter-Island Solar Supply Representative, email 13 May 2013). A detailed list of manufacturer specifications and ratings for modules is available in the Home Power 2012 PV Model Guide. The specifications for the chosen PV panel model were obtained from there.

The average and total PV output potential for the sample set rooftops were calculated by applying the average incoming solar radiation determined by the Area Solar Radiation tool to the Súri formula. When coupled with the total rooftop area, the above formula provides a means to determine the total capacity (kW) and annual energy output (kWh) potential for the study area. These calculations were completed in Microsoft Excel using the exported attribute table from the final rooftop feature class layer. The data outlined in Table 3.6 was added to the rooftop attribute table.

Table 3.6 PV potential calculated data for rooftop layer attribute table

Column	Unit	Description
Average Incoming Solar Radiation in kWh	$kWh/m^2/yr$	1 kWh = 1,000 watts, kWh is the standard unit of energy, calculated by dividing Area Solar Radiation tool results by 1,000.
Total Incoming Solar Radiation on Rooftop	kWh/yr	Average incoming solar radiation multiplied by rooftop area.
Average PV potential per square meter	$kWh/m^2/yr$	Calculated using the chosen equation.
Total Rooftop PV potential	kWh/yr	Average PV potential multiplied by rooftop area.

3.3.5 Statistical Analysis for Extrapolation to Study Area

In order to answer the research question "what is the total solar PV potential for residential rooftops in Kailua Kona," it was necessary to use the data from the sample

set to extrapolate out to the entire study area. To accomplish this, a number of analyses were performed using JMP statistical discovery software. Analysis was done by parcel class and for the total sample set. This work was undertaken to assess the influence of terrain parameters on modeled PV potential and identify the relationship between rooftop and lot size.

Multivariate correlation analysis was performed to identify any simple linear associations between the various terrain parameters, PV potential, rooftop size and lot size. Simple linear regression was run to identify a linear fit equation for rooftop and lot size. This linear fit equation was the basis for extrapolating from the rooftop area in the sample set to estimate the rooftop area in the entire study area.

Multiple linear regression analysis was performed to look at the influence of multiple variables together on PV potential and to build the equations for calculation of total PV potential for study area rooftops. This regression analysis was performed for both average PV potential and total PV potential. The findings from the regression analysis were used to look for patterns between classes and determine the influence of the terrain parameters.

CHAPTER 4: RESULTS

The following chapter shows the results of the modeling efforts described in the methodology as well as a series of statistical analyses. The statistical analysis work was performed to identify relationships and trends in the data in order to extrapolate from the sample parcels to make predictions for PV potential in the entire study area.

4.1 Distribution of Lot Sizes, Rooftop Area, Terrain Parameters, and PV Potential

Table 4.1 displays a summary of the attributes of the total 224 samples parcels (223 in the sample set and one rooftop with real PV production). This layer was created by spatially joining the elevation, slope, and solar radiation point layers to the rooftop polygon layer. Incoming solar radiation was used to calculate PV potential based on the Súri et al. (2005) formula presented in Equation 1 in the literature review chapter. The calculation of PV potential considered the average incoming solar radiation reaching the total rooftop area. The layer was exported to Excel to create a pivot table summary of the attribute characteristics.

In Table 4.1 we see that average elevation is relatively consistent across all classes and in the total sample set. Class 6 displays a significantly higher minimum elevation than all other classes. Minimum, average and maximum slope are also relatively consistent across classes and in the total sample set. Finally, minimum, average and maximum incoming solar radiation and thusly, PV potential, are also consistent across classes and in the total sample set.

Table 4.1 Summary of sample set parcel attributes in six classes: (A)-minimum lot size (m^2), (B)-average lot size (m^2), (C)-maximum lot size (m^2), (D)-minimum rooftop size (m^2), (E)-average rooftop size (m^2), (F)-maximum rooftop size (m^2), (G)-minimum elevation (m), (H)-average elevation (m), (I)-maximum elevation (m), (J)-minimum slope (°), (K)-average slope (°), (L)-maximum slope, (M)-minimum solar radiation (kWh/m^2/yr), (N)-average solar radiation (kWh/m^2/yr), (O)-maximum solar radiation (kWh/m^2/yr), (P)-average PV potential (kWh/m^2/yr), and (Q)-total PV potential (kWh/yr).

	Class 1	Class 2	Class 3	Class 4	Class 5	Class 6	Total
No. of parcels	17	36	59	58	37	17	224
A	554.00	691.00	774.00	958.00	1,423.00	1,896.00	554.00
B	614.47	721.08	879.53	1,114.45	1,576.49	2,263.29	1,114.92
C	685.00	766.00	953.00	1,417.00	1,878.00	2,951.00	2,951.00
D	43.47	109.52	34.67	117.92	195.02	194.65	34.67
E	179.84	227.40	250.49	293.26	324.87	363.62	273.37
F	302.37	452.99	390.74	511.89	489.94	570.05	570.05
G	14.15	29.09	13.21	9.63	6.56	50.36	6.56
H	211.97	182.47	222.36	245.75	205.64	264.85	221.68
I	495.63	525.57	490.81	474.00	526.27	483.08	526.27
J	8.65	9.56	2.04	5.65	11.84	3.68	2.04
K	22.34	20.91	23.48	23.38	22.85	21.76	22.72
L	42.14	38.01	41.11	40.63	38.90	32.60	42.14
M	1,311.25	1,298.06	1,153.50	959.26	1,059.42	1,283.31	959.26
N	1,488.08	1,488.50	1,463.10	1456.87	1,458.92	1,479.98	1,468.06
O	1,642.73	1,662.37	1,658.95	1,626.01	1,666.21	1,636.40	1,666.21
P	158.12	158.17	155.47	154.81	155.03	157.26	156.00
Q	479,093	1,297,527	2,301,597	2,630,450	1,866,895	971,135	9,546,696

On the whole, rooftops in the sample set are approximately one quarter the size of the lots. The total lot size area of the 224 sample parcels is 249,741 square meters and

their digitized rooftop area is 61,234 square meters. When considering rooftop size, both Class 1 and Class 3 show small minimum values (43.47 and 34.67 square meters). There are only two of these small structures in the sample set and they were investigated further. It is likely that they are not in fact residences but rather garage or shed type buildings existing on an empty residential lot. Table 4.1 shows an interesting characteristic for the rooftop area values of Class 2. The classes were stratified by lot size under the assumption that lot size would influence size of homes on it. While the average rooftop sizes fall in line with this assumption, the findings diverge when considering the minimum and maximum rooftop size values. Class 2 has significantly larger values than Class 3, with a minimum of 109.52 and maximum of 452.99 whereas Class 3 has values of 34.67 and 390.74 respectively.

4.2 Correlation Analysis

Multivariate correlation analysis was completed to identify the linear association between PV potential and each explanatory variable in order to test for any relationship between the variables. Correlations were assessed by class section and across all samples. Results are displayed in Tables 4.2 and Table 4.3.

In Table 4.2, we can see that average PV potential per square meter is the most strongly correlated with average slope across all classes. This negative relationship indicates a lower PV rooftop solar photovoltaic potential on more steeply angled surfaces.

Table 4.2 Standard correlation showing the relationship between variables across all classes: (A)-average PV potential (kWh/m2), (B)-average elevation (m), (C)-average slope (degrees), (D)-size of rooftop (m^2), and (E)-lot size (m^2)

Class		A	B	C	D	E
Class 1	A	1.00				
N = 17	B	0.12	1.00			
	C	**-0.85**	**-0.02**	1.00		
	D	**-0.34**	0.34	0.10	1.00	
	E	**-0.35**	0.47	0.23	0.15	1.00
Class 2	A	1.00				
N = 36	B	0.12	1.00			
	C	**-0.83**	0.10	1.00		
	D	0.13	**-0.06**	**-0.26**	1.00	
	E	**-0.17**	0.26	0.35	**-0.28**	1.00
Class 3	A	1.00				
N = 59	B	0.11	1.00			
	C	**-0.81**	**0.04**	1.00		
	D	0.09	**0.01**	**-0.06**	1.00	
	E	**-0.05**	**-0.03**	0.14	0.20	1.00
Class 4	A	1.00				
N = 58	B	0.12	1.00			
	C	**-0.75**	0.24	1.00		
	D	**-0.60**	**-0.04**	0.04	1.00	
	E	**-0.07**	**-0.17**	0.13	0.07	1.00
Class 5	A	1.00				
N = 37	B	**-0.03**	1.00			
	C	**-0.91**	0.15	1.00		
	D	0.10	**-0.05**	**-0.24**	1.00	
	E	**-0.02**	0.26	**0.00**	0.28	1.00
Class 6	A	1.00				
N = 17	B	**-0.03**	1.00			
	C	**-0.93**	0.13	1.00		
	D	**-0.07**	0.35	0.12	1.00	
	E	**-0.02**	**-0.24**	0.15	0.29	1.00

Bold indicates statistically significant (0.99)

The correlation between average PV potential with rooftop size or lot size is not as clear. Class 1 and Class 4 samples display the strongest statistically significant correlation between rooftop size and average PV potential (-0.34 and -0.60). Class 1 also shows a negative correlation between lot size and PV potential (-0.35) which is also statistically significant. Both of these correlations are negative suggesting that larger rooftops and lot sizes have less average PV potential per square meter. Class 2, 3, and 5 rooftop size is positively correlated with PV potential while lot size is negatively correlated; however only lot size shows significance.

Elevation appears to show a slightly positive correlation with rooftop size (0.34) and lot size (0.47) in Class 1, which suggests that larger lot sizes are located in higher elevation areas. It is not statistically significant, however. In Class 2, average elevation shows a small correlation (0.26) with lot size. Class 5 shows the same correlation between lot size and elevation (0.26), also suggesting that larger lot sizes appear to be located at higher elevations but neither are statistically significant. This is not, however, the case for Class 6 where elevation and lot size show a statistically significant negative correlation. Class 6 does display a moderate correlation between rooftop size and elevation (0.35), although it is not significant.

When looking at the relationship between rooftop and lot size, all classes display a positive relationship except Class 2 which is the only statistically significant variable. Class 3, 5 and 6 show a moderate correlation between rooftop and lot size (0.20, 0.28 and 0.29, respectively) with no statistical significance. This suggests that larger lot sizes have larger homes. The remaining classes (1 and 4) show little correlation between these two variables.

Table 4.3 displays the correlation across all samples. We can see that average PV potential per square meter is strongly correlated with average slope (-0.83) with statistical significance, while no significant correlation is shown with elevation. Average PV potential is not very correlated with rooftop area or parcel area but the relationship is statistically significant. Lot size and rooftop appear to be relatively correlated (0.54) with statistical significance. This warrants further investigation into the relationship between rooftop and lot size as this relationship will be used to estimate the total available rooftop space for the study area.

Table 4.3 Standard correlation table showing the relationship between variables across all 224 samples. (A): average PV potential (kWh/m^2), (B): average elevation (m), (C): average slope (degrees), (D): size of rooftop (m^2), and (E): lot size (m^2).

N = 224	A	B	C	D	E
A	1.00				
B	0.07	1.00			
C	**-0.83**	0.12	1.00		
D	**-0.03**	0.08	**-0.03**	1.00	
E	**-0.04**	0.07	**0.03**	**0.54**	1.00

Bold indicates statistically significant (0.99)

When considering the results of the above multivariate correlation analyses, one consistently sees a strong negative correlation between PV potential and average slope. The findings from the multivariate correlation for both the total samples as well as the correlations at each Class level show there is not much significant interaction between the elevation and slope variables. Thus, we can further investigate how they influence PV potential without being concerned about how they may be affecting one another.

The relationship between lot size and rooftop area is of particular interest in this study as total rooftop area must be estimated based on lot size data. The correlation

analysis results are inconclusive. The total sample set shows a statistically significant correlation of 0.54 (Table 4.3) but when considered by class there are no consistent findings. Class 2 shows a significant negative correlation of -0.28 and Class 4 does not display any significant correlation at 0.07.

4.3 Rooftop and Lot Size Correlation

In order to estimate the total residential rooftop photovoltaic potential for the study area it is necessary to extrapolate from the sample set results. For the sample, 224 parcels (223 samples and one rooftop with real PV production) were chosen for rooftop digitizing from the total of 4,460 residential parcels in the study area. The relationship between rooftop and lot size was analyzed using a bivariate fit Y by X model. The bivariate fit model provides the intercept and coefficient for the linear fit of rooftop to parcel size. The results are displayed in Table 4.4. The intention was to use the findings in order to estimate the total rooftop area in the 4,460 residential parcels. Similar to the multivariate correlation discussed in Section 4.2, there is little conclusive when considering the samples broken down by Class. The adjusted R^2 values for Classes 1-6 show no significant influence of lot size on rooftop area. Once again we see a negative coefficient relating rooftop size and lot size for Class 2. When considering the total sample set, we see a more promising adjusted R^2 value of 0.29.

Table 4.4 Bivariate fit modeling the correlation between rooftop and lot size for each Class 1-6 and the total sample set

	Class 1	Class 2	Class 3	Class 4	Class 5	Class 6	Total
R^2_{Adj}	-0.04	0.05	0.02	-0.01	0.05	0.02	0.29
Intercept	46.74	836.96	65.55	258.66	66.65	155.18	**162.14
Coefficient	0.22	-0.85	0.21	0.03	0.16	0.09	**0.10

**statistically significant 0.99

4.4 Regression Analysis

After reviewing the results from the multivariate correlations and the simple linear regression, a final analysis was run to look at the influence of the multiple variables together and build the linear fit equation that would be used for extrapolation to the entire study area. Multiple linear regression was used to identify the relationship between the slope, elevation, rooftop area and lot size explanatory variables and their influence on the modeled PV potential values. This method was employed so that a stronger case could be made for the findings from the modeling exercise. The results discussed here serve as the basis to the extrapolation to the entire study area. Both standard least squares and stepwise approaches were utilized. Each method displayed the same final results. Table 4.5 displays the results for average PV potential and Table 4.6 summarizes the results for total rooftop PV potential.

Table 4.5 Average PV potential least squares regression analysis (A)-average PV potential ($kWh/m^2/yr$) from ESRI model, (B)-average elevation coefficient, (C)-average slope coefficient, (D)- rooftop area coefficient and (E)- lot size coefficient

	**Class 1	**Class 2	**Class 3	**Class 4	**Class 5	**Class 6	**Total
A	158.12	158.17	155.47	154.81	155.03	157.26	156.00
R^2_{Adj}	0.86	0.72	0.66	0.64	0.84	0.86	0.71
Intercept	**234.51	**163.92	**174.54	**177.39	**206.81	**170.54	**188.18
B	0.03	0.01	0.01	0.03	0.01	0.01	0.01
C	**-1.09	**-1.31	**-1.37	**-1.56	**-1.88	**-1.31	**-1.44
D	*-0.08	0.03	0.01	0.01	-0.00	0.00	0.00
E	*-0.06	-0.01	0.00	-0.00	-0.02	-0.01	-0.01

*statistically significant 0.95
**statistically significant 0.99

In Table 4.5 we see that the average slope was the most statistically significant variable across all classes and in the total sample. Elevation also shows a significant

influence when considering the total sample set. Class 1 shows some statistically significant influence from both rooftop area and lot size but this is not seen in any of the other classes nor does it appear this way for the total sample set. Overall, rooftop and lot size show very little influence on average PV potential per square meter in the linear fit equation.

The adjusted R^2 values for each class range from 0.67 in Class 3 up to 0.84 in Class 4. Here we see an adjusted R^2 value of 0.71 for the total sample set indicating that the variables included can describe approximately 71 percent of the variance in PV potential.

Table 4.6 Total PV potential least squares regression analysis (A)-total PV potential (kWh/ yr) from ESRI model, (B)-average elevation coefficient, (C)-average slope coefficient, (D)-roof top area coefficient, and (E)-lot size coefficient

	**Class 1	**Class 2	**Class 3	**Class 4	**Class 5	**Class 6	**Total
A	479,093	1,297,526	2,301,596	2,630,449	1,866,895	971,135	9,546,696
R^2_{Adj}	0.99	0.99	0.98	0.97	0.97	0.99	0.98
Intercept	*11,182.44	1,981.36	3,430.38	*6,900.85	*14,942.77	999.92	**7,738.05
B	*7.65	*2.33	*3.71	*7.72	4.72	4.44	**3.83
C	**-174.06	**-269.96	**-289.47	**-456.59	**-616.61	**-462.06	**-385.18
D	*150.86	**161.14	**160.90	**154.30	**153.30	**157.73	**157.05
E	-12.80	3.65	1.41	1.77	-0.74	3.38	-0.13

* statistically significant 0.95
**statistically significant 0.99

As one would expect in Table 4.6, rooftop area plays a significant role in total rooftop PV potential. Here we see slope as the other significant variable across all classes and elevation once again statistically significant for the entire sample set. The adjusted R^2 values for total PV potential least squares regression range from a low of 0.97 in Class 5 to 0.99 in Classes 1 and 2. The total sample set has an adjusted R^2 of 0.98.

4.5 Extrapolation to Study Area: Rooftop Area, Average and Total PV Potential

In order to answer the proposed research question, it was necessary to use the rooftop lot size bivariate fit equation built from the sample set data (Table 4.4) along with the regression equations created for the average and total PV potential (Tables 4.5 and 4.6) and apply them to the data available for the entire study area parcels. The first step was to estimate the total rooftop area for all residential parcels. This was done using the equations built from the coefficients in Table 4.4 and the results are displayed in Table 4.7. The rooftop area for each of the 4,460 was calculated using the lot size area listed in the TMK parcel dataset. The available data shows total lot area equaling 4,959,217.49 square meters. In Column B of Table 4.7 there are two rooftop totals listed for the study area. The sum of classes total is the total rooftop area as summed from the bivariate fit equations for each class. The second total was calculated using the bivariate fit equation built for the total sample set. The results from the calculations performed here estimate total rooftop area between 1,213,074.61 and 1,219,066.15 square meters, or approximately 24.5 percent of lot area. This falls in line with the sample set measured values discussed in Section 4.1.

This estimated rooftop area was then utilized for the average and total PV potential equations. Table 4.7 also displays the results for average and total PV potential for the study area. The average rooftop PV potential per square meter was calculated for the study area based on the linear fit equations built from the regression analysis displayed in Table 4.5. Total PV potential was calculated using the equations built from Table 4.6. For both calculations, the average elevation and slope variables were

populated using the sample set average values calculated for each class (displayed in Table 4.1).

Table 4.7 shows the total PV potential using the regression analysis equations. Here we see a range of 189.847,428 - 190,788,394 kWh (or 189.85-190.79 GWh) of electricity annually.

Table 4.7 Regression analysis rooftop area, average and total PV potential: (A)-Total lot area from parcel data (m^2), (B)-total calculated rooftop area (m^2), (C)-average calculated PV potential (kWh/m^2/yr), and (D) total PV potential (kWh/yr)

	A	B	C	D
Class 1	212,453.91	62,471.29	159.11	9,234,300.24
Class 2	509,134.07	158,830.50	158.28	25,176,164.25
Class 3	1,023,162.68	292,103.62	155.40	45,466,573.85
Class 4	1,319,884.01	344,389.50	154.89	53,281,471.12
Class 5	1,103,117.98	227,609.66	155.11	35,357,562.85
Class 6	791,464.85	127,670.03	157.13	20,031,420.68
Total (sum of classes)	4,959,217.49	1,213,074.61	156.65	189,847,428.76
Total (regression analysis)	4,959,217.49	1,219,066.15	156.10	190,788,394.32

When considered in the context of the total energy use by Hawaii Island, this is approximately 17 percent of the total electricity HELCO provided to the Island in 2012. At the current residential electricity rate of $.43, the total of 190.79 GWh per year has a dollar value of value of $82,039,009.56. This works out to be an average of 42,778 kWh or $18,394 per rooftop. This potential far exceeds the average demand for an average household. Typical residential energy use is around 500 kWh per month or approximately $2,580 dollars for electricity annually (DBEDT 2013a). These findings are elaborated on in the discussion chapter.

4.6 Comparison with Real Home PV Production

One parcel from the sample set was chosen for comparison with modeled findings. This parcel is in Class 5 with a total lot size of 1,673 square meters. The digitized rooftop area measures 340.92 square meters. This digitized rooftop area was compared to the rooftop area calculated by applying the bivariate fit equations built from Table 4.4. When using the Class 5 equation with the given lot size, the rooftop area for this parcel calculates out to be 340.76 square meters. This is very close to the digitized area. The bivariate fit equation for the total sample set calculates a rooftop area of 329.48 square meters.

The modeled average PV potential generated by this study using the Esri toolset was analyzed against actual generation data recorded by the homeowner's PV tracking system. It is important to note that the PV potential values initially calculated using the modeled incoming solar radiation were based on the SW260 panel chosen for this research and presented in the methods section. After discussing with the homeowner however, it was discovered that he does not have the SW260 installed, and the characteristics associated with the installed panel are quite different. The main thing to note is that the installed panel is both smaller and less powerful than the SW260 used in the original calculations. The estimated PV potential from the incoming solar radiation model was adjusted to properly reflect the installed panel's size and power rating in order to accurately compare with the real time product data collected from the home. Table 4.8 below shows how the installed panels compare with the type used for the original estimation.

Table 4.8 Solar panel information used for model versus as built on sample home

	Originally Modeled	Modified to As Built
Panel Type	Solar World SW260	Solar World SW175
Total rated power output in W per m^2 (PTC or PV USA conditions, unit-W)	232.30	156.60
Panel size (m^2)	1.68	1.34
Panel output (kW/m^2)	0.14	0.12
Average Solar Radiation from Esri model (kWh/m^2/year)	1,568.78	1,568.78
Average PV Potential (kWh/m^2/yr)	166.70	145.06
Total Rooftop Area (m^2)	340.92	340.92
Total PV Potential (kWh/yr)	56,832.27	49,453.47

The actual generation data from the site was downloaded from the Enphase Enlighten dashboard system with the homeowner's permission. Production data was collected for all of 2012 and from January 1, 2013 to June 30, 2013. There are a total of 12 panels on the rooftop but only 11 were functioning during 2012. Calculations were adjusted to reflect the installed panel type and the difference in total panel area between 2012 and 2013. Because data for 2013 was only available through June, the total output for the six months was doubled to get an estimate for the entire year. The total PV production in 2012 and estimated total for 2013 was used to calculate the average PV production per square meter. This recorded average PV potential was then compared with the modeled average PV potential. The results are displayed in Table 4.9.

When we compare the recorded PV production with the model we see the adjusted model average PV potential significantly underestimated the actual PV generation per square meter. The study modeled average PV potential of 145.06 kWh/m^2/yr is 68 percent of the actual production in 2012 (212.5 kWh/m^2/yr) and 69 percent of the average estimated for 2013 (208.48 kWh/m^2/yr). When taking this

difference into account it is important to remember that the model assumed an average for the entire rooftop incoming solar radiation whereas the 12 panels on the home were installed on the portion of the roof receiving the most sun. This discrepancy is addressed in more detail in the discussion chapter.

Table 4.9 Recorded rooftop PV production data compared with adjusted model

	Actual 2012	Actual 2013	Adjusted Model
Logged PV Production 6 months January - June (kWh)	1,597.34	1,631.28	
PV Production 12 months (kWh)	3,043.27	*3,262.57	
Total PV Panel Area (m^2)	14.35	*15.65	
PV Production (kWh/m^2/yr)	212.15	*208.48	145.06

*estimate based on 6 months data

CHAPTER 5: CONCLUSION AND DISCUSSION

This study sought out to answer the question: What is the PV potential for residential rooftops in Kailua Kona? This work provides a high level overview of photovoltaic energy potential in the study area and proposes a method to model two pieces of information that were unavailable at the time the study was implemented. These include high-resolution incoming solar radiation data and total rooftop area. The work highlights the potential for future analysis using LiDAR data to automate rooftop inventories and describe solar radiation point data on rooftops.

Based on the total study area regression analysis findings presented in this document (Table 4.7), we see that the estimated photovoltaic electric energy generation potential for rooftops is approximately 190,000,000 kWh annually. This would be approximately 17 percent of the total electricity the utility provided to the entire Big Island in 2012 (DBEDT 2013a).

While it is not possible to calculate exact installed capacity for the proposed energy generation, we can make an estimate based on calculated rooftop area. For example, total rooftop area from the sum of each class equals 1,213,075 m^2. This amount of space could potentially hold up to 722,068 Solar World SW260 PV panels (each panel is 1.68 m^2). This equates to 129,157 kW or approximately 130 MW in distributed PV capacity (with standard derating of 0.77). Installations of this magnitude would be about 36 percent of the utility's current total generating capacity and 69 percent of the Big Island's peak load (DBEDT 2013a).

When reporting these PV potential and rooftop area estimates, it is essential to discuss the uncertainty inherent in these findings. Three main steps were taken to build

the model for extrapolation to the study area. It was first necessary to select a representative sample, then the linear fit between rooftop size and lot size was calculated, and finally multiple linear regression analysis for total PV potential was completed. Uncertainty was introduced at each step in the analysis and is discussed in detail in the next paragraphs.

A total of 4,460 residential parcels were identified within the study area. Recognizing that digitizing and calculating incoming solar radiation for each rooftop was not feasible, a 5 percent sample set (223) was chosen to provide the basis for extrapolation. This sample size has a 95 percent confidence level with confidence interval of 6.4. This means that we can be 95 percent confident that a sample size of 223 parcels (+/- 6.4) will provide accurate representation of parcels in the whole study area.

The total rooftop area was predicted using the bivariate fit Y by X model. The sample rooftop areas were fit against the lot sizes and these equations were the basis for extrapolation to the entire study area. This model explains about 30 percent of the variability in rooftop area across the study area according to adjusted R^2 .

The multiple linear regression model predicts total PV potential based on average elevation, average slope, rooftop area and lot size. This has a higher degree of confidence with an adjusted R^2 of 0.98. The model therefore can describe almost all of the variation in PV potential in the sample rooftops. That said, this model is inextricably linked to the available rooftop area thus relies on the input from the less certain bivariate fit model.

Beyond the statistical uncertainty there are also unquantified sources of uncertainty introduced by processing of LiDAR point data, manual digitization of rooftops, estimating solar radiation, and averaging of parameters for calculation of PV

potential. While great care was taken to minimize errors, it is important to recognize potential sources of uncertainty introduced throughout the research. Additionally, there were a number of simplifications that were necessary to complete the analysis. These are described in the next section.

5.1 Project Assumptions

The findings presented in this document are based on a methodology that has simplifications about system design and overall feasibility. The regression equations utilized were constructed using averages for each rooftop as opposed to individual point data. The research was designed as such to overcome inconclusive point data and produce an understanding of the overall potential magnitude of distributed rooftop PV in this region. The hope is that this work can inform future research projects that further integrate higher resolution topographic data and imagery to create viable solar insolation point data for individual homeowners. The major assumptions are described in detail in this section in order to set the stage for evaluating the methodology and describing future research.

For this study it was assumed that the entire rooftop can be used for PV generation. Based on the extrapolated total rooftop calculations, average rooftop area for the 4,460 parcels in the study area is approximately 272 m^2. An average rooftop of this size could hold approximately 161 panels per rooftop, or a 28.76 kW system (with standard derating of 0.77). DBEDT (2013a) estimates the current residential PV systems on Hawaii Island around 4.4 kW per system. The national average for residential is 4.77 kW (IREC 2013). Thus, the average whole rooftop system proposed by this project would be at least six times the current average size.

In reality, whole roof PV installations are not feasible. The major limiting factors include grid saturation and high installations costs. In the systems described here, production capacity far outweighs typical household usage. Current residential usage is approximately 500 kWh per month or 6,000 kWh annually (DBEDT 2013a). This study's findings estimate the overall PV potential energy generation around 190,000,000 kWh (190 GWh). This would be approximately 42,600 kWh per rooftop; over seven times the current usage. Based on these findings, full rooftop PV installations on the study area homes could provide enough energy to power over 31,000 homes annually.

As discussed in the introduction chapter, grid interconnection is a very important consideration. Whenever generation is greater than what is being consumed the power must go somewhere. Solar electricity is not a firm source of power and therefore is only available during daylight hours and at varying intensity throughout the day. The fact that an excess of generation would be produced during a short period of time during the day would cause substantial interconnection issues that would need to be addressed before any installations of such magnitude could be considered. With high levels of distributed PV generation already causing saturation issues on much of the utility grid, the oversizing of rooftop systems is even less likely in the future.

The research design also does not consider financial feasibility of installations of this size. There are high installation costs associated with the larger system sizes like those proposed here. If we are to take the proposed system size of 28.76 kW and look at overall cost of installation based on current installed costs of about $5,750 per kW, each household system would cost approximately $165,370 before rebates and tax credits (Solar Energy Industry Association 2012; DBEDT 2013a). Even with available tax

credits and incentives potentially reducing installed cost by over 50 percent, this would still be a tremendous investment. Without a system to sell power back for distribution, systems of this size would not make financial sense for homeowners.

Despite these simplifications and assumptions there is some value in the methods developed for this study. The following sections discuss the methods in detail to identify the strengths and weaknesses of the work undertaken.

5.2 Review of Methodology

The methods were designed to overcome a lack of available data for the study area. The main things executed in this research include (1) modeling solar radiation, (2) estimating available rooftop area and (3) calculating PV from incoming solar radiation. The high resolution LiDAR data was a key input for the completion of this study.

5.2.1 LiDAR Performance

LiDAR was chosen as the main source data for the rooftop analysis performed in this study. This decision was made to take advantage of the benefits of using the highest resolution data available. As explained by Chen (2007), LiDAR is gaining popularity in many urban planning and landscape ecology applications.

The ArcGIS 3D Analyst extension was used to process the point clouds to usable products for the study. The LiDAR data obtained contained raw ASCII files with all points, ground, points and extracted points. The extracted points were chosen to create the 2-meter resolution digital surface model (DSM). Thus, the final surface included all the extracted points, meaning both the building rooftops and surrounding vegetation are displayed in the surface model.

The inclusion of both vegetation and rooftop points proved more problematic than originally anticipated. Because the rooftop points could not be differentiated from the surrounding vegetation automatically, the building rooftops had to be manually digitized to isolate rooftop points. This greatly increased the time needed to generate a rooftop sample and introduced additional human error into the sample as well.

The DSM served as the main source data for the rooftop elevation, slope, aspect, and solar radiation data points. These point datasets were clipped to the rooftop sample to prepare for spatial joining. Figure 3.8 displays highly divergent solar insolation points that warranted additional review to determine the reliability of these results. Using the aspect points (Figure 3.9) and a high resolution image obtained from Google Earth (Figure 3.10), it was determined that there were some significant limitations in the point data as it was displayed on rooftops. In particular, the orientation (aspect) points do not appear to align with the as-built rooftop directions. This error could have been introduced during processing or digitizing, but it also could be a result of the age of the LiDAR data. For example, the image displayed in Figure 3.10 was captured in 2013 while the LiDAR points were collected in 2006. The differences in rooftop appearance and LiDAR points could also be attributed to modifications made to the vegetation and building structures during the seven years between the times when the different datasets were created.

5.2.2 Modeling Solar Radiation

As discussed in the previous section, great care was taken to utilize existing high resolution LiDAR data and build a 2-meter digital surface model as the input to calculate solar radiation. Because of the high resolution of this input data, processing time for calculating incoming solar radiation greatly increased. Insolation calculations are

typically very time-consuming, especially with high-resolution topographic data. Like any research project, trade-offs must be made between accuracy and calculation time. After an initial effort to run the area solar radiation with a higher resolution values for the viewshed (sky size) and day interval, it was determined this resulted in significant calculation time that was not feasible with the computer available for processing. To overcome this barrier, the default input values for the Area Solar Radiation tool were chosen. Although the default value for viewshed is adequate for complex topography, the output solar radiation surface could have benefited from optimizing input parameters for surfaces with man-made structures.

5.2.3 Rooftop Area Estimation

At the outset, this study suffered from the lack of a rooftop or building structure dataset. The available parcel dataset only included lot size measurements. The methodology was then developed to test the hypothesis that lot size was in some way correlated with rooftop size in the sample set with the hope that the available parcel dataset could be utilized to predict rooftop area for the sample set.

The residential parcels were divided into classes by area in order to select the representative sample randomly. Rooftop size was digitized for all parcels in the sample set and the parcel with real time PV production. These rooftop sizes were then analyzed against the lot sizes to develop the bivariate fit equation for each class and across the entire sample set. The intention was to evaluate the performance of the model at each class level compared with the equations built for the total sample set to see if the division into classes showed any additional correlations that were not visible when analyzing the sample as a whole. Similar to the work completed by Wiginton et al. (2010), these

equations were used for extrapolation to the study area. The correlation between rooftop and lot size is displayed in Table 4.4.

The adjusted R^2 values for these correlations did not initially offer much confidence in the fit model built for Classes 1 to 6, respectively, thus indicating very little association between rooftop and lot size. The equation built for the total sample set shows an adjusted R^2 of 0.29, offering a bit more confidence in the relationship but still only indicating that parcel size can explain approximately 30 percent of the variance in rooftop size.

When designing this research project, the initial intention was to have at least two parcels for a ground truth comparison with modeled data. Unfortunately, after contacting multiple residents, only one homeowner with at least one year of historical data was willing to volunteer this information. This parcel is located in Class 5. For this chosen parcel, digitizing produced a feature class with rooftop size of 340.92 m^2. When the Class 5 bivariate fit equation is applied to the parcel size, the rooftop area calculates to be 340.76 m^2. The total sample set bivariate equation calculates this rooftop to be 329.48 m^2. This indicates that despite the low adjusted R^2, the Class 5 fit model was more effective at predicting the rooftop area for this particular parcel. Further assessment of the calculated rooftop areas for each of the 223 digitized samples would provide additional insight into the error associated with the fit models created by class and for the entire sample set.

5.2.4 Estimating PV Potential

This study was designed by averaging incoming solar radiation for each rooftop and then using that value to predict average PV potential. This means that the entire

rooftop, including portions that had lower incoming solar radiation, were also included in the analysis. The method employed here was implemented as a means to overcome uncertainty displayed in the specific rooftop point data (Figure 3.8, Figure 3.9).

We see the effects of the averaging when we compare the model findings with the home with real PV production data. Table 4.9 shows a significant difference between the average PV potential ($kWh/m^2/yr$) produced on the actual rooftop installation in 2012 and 2013, and the average predicted by our project model. The average predicted PV potential from the model is 30 percent less than the average PV produced by the installed panels. The homeowner has installed a smaller system that is strategically located on the portion of the rooftop receiving the most sunlight. Therefore the average energy produced is justifiably higher than our predicted average for the entire rooftop.

That being said, the PV potential estimated for the sample set rooftops is based on the incoming solar radiation and the efficiency of the technology installed on the roof. Since it was possible to adjust the model for the specific type of panel installed on this rooftop, this discrepancy could also be the result of the input parameters chosen for the solar radiation toolset.

5.3 Future Research

This study was designed as a starting point to assess PV potential in an area that has not yet had an analysis of this sort. It is useful to have an idea of the total potential PV production but it does not provide an in depth analysis of the feasibility of the installation of this magnitude of rooftop PV. There were many simplifying assumptions that were made in order to move forward with this work and while we were able to

answer the research question, a number of new research directions have been identified since performing this work.

5.3.1 LiDAR

The use of LiDAR point data offers a major opportunity for future research in both automating rooftop inventories and calculating incoming solar radiation and PV potential for homeowners. The results of the point data produced for rooftops in this study highlight some uncertainty in the LiDAR surface created (Figure 3.8, Figure 3.9). In the near term, future research is needed to improve the reliability of the rooftop point data. Specifically, efforts to isolate vegetation from rooftop points are necessary.

Chen (2007) is a proponent for using imagery to validate filtering results from LiDAR. In this case, analyzing additional rooftops against available imagery could assist in the differentiation of trees from building structures. Even without high cost processing software, there are opportunities to use existing imagery to automate the creation of a rooftop vector layer. The Solar Model for the County of Los Angeles Solar Mapping Portal (2010) uses aerial imagery to derive a normalized difference vegetation index (NDVI) to subtract from the digital surface model to isolate buildings. The benefits for automating rooftop layer creation are especially relevant for the Big Island, where there is a lack of building structure data. The ability to create quick and low cost rooftop solar inventories for whole communities would help developers and future homeowners optimize the installation of photovoltaic technologies.

Future photovoltaic modeling should move beyond the use of averages, using the technique described and implemented to get point data in this study. Averaging was a necessary first step but it has identified the need for more detailed areas that need be

explored further for the data to become more useful in a real world implementation. By generalizing the terrain parameters this study has done little to identify areas that would be more appropriate to focus on for PV. This would also allow the incorporation of aspect points which would add another significant variable to the overall analysis. In the face of major grid saturation issues, solar radiation point data would give homeowners an idea about viable areas for panel placement and better inform on the overall installation costs and therefore the return on investment.

5.3.2 Optimizing Solar Radiation Model

With more time, additional optimization of the solar radiation model input parameters would be beneficial. Multiple solar radiation surfaces should be created to test performance. By optimizing the input parameters for a finer resolution viewshed one may see more accurate results for complex surfaces with man-made structures. Modeled surfaces could also be analyzed against measured incoming solar radiation collected from a local weather station throughout the year. Although, at the time of this research was conducted, only one weather station existed within in the area where LiDAR data was collected.

REFERENCES

AWS Truepower, Inc. 2013. Resource Assessment. http://www.awstruepower.com/solutions/solar/resource-assessment/ (last accessed 27 November 2013).

Braccio R, P. Finch, and R. Frazier. 2012. Hawaii clean energy initiative scenario analysis: Quantitative estimates used to facilitate working group discussions 2008-2010. National Renewable Energy Laboratory. http://www.hawaiicleanenergyinitiative.org/storage/pdfs/Hawaii Clean Energy Initiative Scenario Analysis_March 2012.pdf (last accessed 1 April 2013).

Chaves A, and A. Terry. 2010. Locating sites for photovoltaic solar panels: Pilot study uses DEM derived from LiDAR. *ArcUser* 2010: 24-27.

Chen, Q. 2007. Airborne lidar data processing and information extraction. *Photographic Engineering and Remote Sensing* 73: 109-112.

Choi Y, J. Rayl, C. Tammineedi, and J. Brownson. 2011. PV Analyst: Coupling ArcGIS with TRNSYS to assess distributed photovoltaic potential in urban areas. *Solar Energy* 85: 2924-293.

Clark D, S. Klein, and W. Beckman. 1984. A method for estimating the performance of photovoltaic systems. *Solar Energy* 33 (6): 551-555.

Creative Research Systems. 2012. Sample size calculator. http://www.surveysystem.com/sscalc.htm - two (last accessed 3 April 2013).

Davies, M, C. Gagne, Z. Hausfather, and D. Lippert. 2007. Analysis and recommendations for the Hawaii county energy sustainability plan. http://www.kohalacenter.org/pdf/analysis_and_recommendations.pdf (last accessed 28 October 2013).

Dubayah, R, and P. Rich. 1995. Topographic solar radiation models for GIS. *International Journal of Geographic Information Systems* 9 (4): 405-419.

Esri. 2013a. ArcGIS Help 10.1. Area Solar Radiation (Spatial Analyst). http://resources.arcgis.com/en/help/main/10.1/index.html#//009z000000t5000000 (last accessed 31 October 2013).

Esri. 2013b. ArcGIS Bing Maps Aerial. http://www.arcgis.com/home/item.html?id=25c3f49d4ce3451e8a7f5b5aebccab48 (last accessed 23 May 2013).

Esri. 2013c. ArcGIS Help 10.1 Spatial Join (Analysis). http://resources.arcgis.com/en/help/main/10.1/index.html#//00080000000q000000 (last accessed 2 February 2013).

Fu, P, and P. Rich. 1999. Design and implementation of the Solar Analyst: An ArcView extension for modeling Solar Radiation at Landscape Scales." In Proceedings of the Nineteenth Annual ESRI User Conference. San Diego, California. http://proceedings.esri.com/library/userconf/proc99/proceed/papers/pap867/p867.htm (last accessed 22 December 2012).

Global Energy Concepts. 2006. A Catalog of Potential Sites for Renewable Energy in Hawaii. http://state.hi.us/dlnr/reports/LD07-Hawaii Renewable Energy Development Catalog.pdf (last accessed 19 December 2012).

Hawaii Clean Energy Initiative (HCEI). 2010. Hawaii Clean Energy Initiative http://www.hawaiicleanenergyinitiative.org/ (last accessed 30 October 2013).

Hawaii Clean Energy Initiative (HCEI). 2011. Hawaii Clean Energy Initiative Roadmap. http://www.hawaiicleanenergyinitiative.org/storage/media/HCEI%20RoadMap_2011_40pgs.pdf (last accessed 30 October 2013).

Hawaii Electric Company (HECO). 2013. Net Energy Metering in Hawaii. http://www.heco.com/heco/Clean-Energy/Clean-Energy-Generation/Net-Energy-Metering-in-Hawaii#bk1 (last accessed 10 November 2013).

Hawaii Electric Light Company (HELCO). 2013. Solar integration policy changes. http://www.helcohi.com/portal/site/helco/menuitem.b136fe8120a5c28884276c10c510b1ca/?vgnextoid=0c809cb2ab721410VgnVCM10000005041aacRCRD&cpsextcurrchannel=1 (last accessed 20 November 2013).

Hawaii Natural Energy Institute. 2012. PV Test Beds in the Micro-Climates of Hawaii. University of Hawaii at Manoa: Hawaii Natural Energy Institute: School of Ocean and Earth Science and Technology. http://www.hnei.hawaii.edu/projects/photovoltaic-test-beds-micro-climates-hawaii (last accessed 29 December 2013).

Helios Environmental Modeling Institute, LLC. 2000. The Solar Analyst 1.0 User Manual. http://www.precisionviticulture.com/files/fu_rich_2000_solaranalyst.pdf (last accessed 29 December 2013).

Helm, C, and K. Burman. 2010. Kauai, Hawaii: Solar resource analysis and high-penetration PV potential. Golden, Colorado: National Renewable Energy Laboratory, Report Number, NREL/TP-7A2-47956.

Herbst, D. 2009. Solar mapping: demystifying solar potential. *Renewable Energy Focus* 10 (4): 32-35.

Hetrick, W, P. Rich, and S. Weiss. 1993. Modeling insolation on complex surfaces. Proceedings of the Thirteenth Annual ESRI User Conference. 2: 447-458. http://professorpaul.com/publications/hetrick_et_al_1993_esri.pdf (last accessed 29 December 2013).

Hofierka, J, and J. Kanuk. 2009. Assessment of photovoltaic potential in urban areas using open-source solar radiation tools. *Renewable Energy* (34): 2206-2214.

Home Power. 2012. 2012 PV Module Guide. https://homepower.com/articles/2012-pv-module-guide (last accessed 4 March 2013).

International Building Performance Simulation Association. 2011. Solar Radiation Components. http://www.bembook.ibpsa.us/index.php?title=File:Solar_radiation_components.png (last accessed 30 December 2013).

Interstate Renewable Energy Council (IREC). 2013. Annual Updates and Trends Report. http://www.irecusa.org/wp-content/uploads/2013/10/IREC-Trends-Report-2013-Web-1.pdf (last accessed 10 November 2013).

Izquierdo, S, M. Rodrigues, and N. Fueyo. 2008. A method for estimating the geographical distribution of the available roof surface area for the large-scale photovoltaic energy-potential evaluations. *Solar Energy* 82: 929-939.

Jakubiec, A, and C. Reinhart. 2012. Towards validated urban photovoltaic potential and solar radiation maps based on LiDAR measurements, GIS data, and hourly DAYSIM simulations. Cambridge, MA: Building Technology Program, Massachusetts Institute of Technology. http://web.mit.edu/SustainableDesignLab/publications/SimBuild2012_jakubiec,reinhart_towards-validated-urban-solar-radiation-maps.pdf (last accessed 29 December 2012).

Jo, J, and T. Otanicar. 2011. A hierarchical methodology for the mesoscale assessment of building integrated roof solar energy systems. *Renewable Energy* 36: 2992-3000.

Kang, S, S. Kim, and D. Lee. 2002. Spatial and temporal patterns of solar radiation based on topography and air temperature. *Canadian Journal of Forest Research* 32 (3): 487-497.

Katiyar, A, and C. Pandey. 2013. Review of solar radiation models- part 1. *Journal of Renewable Energy* 1-11.

Kerschen, M. 2012. County level analysis of residential solar adoption in the US. Master's thesis, Boulder, CO: Colorado State University.

Knier, G. 2011. How do photovoltaics work? http://science1.nasa.gov/science-news/science-at-nasa/2002/solarcells/ (last accessed 28 December 2013).

Kumar, L, A. Skidmore, and E. Knowles. 1997. Modelling topographic variation in solar radiation in a GIS environment. *International Journal of Geographical Information Science* 11(5): 475-497.

Leitelt, L. 2010. Developing a Solar Energy Potential Map for Chapel Hill, NC. Master's thesis, Chapel Hill, NC: University of North Carolina.

Los Angeles County. 2010. Developing the solar model for the County of Los Angeles solar mapping portal. http://egis3.lacounty.gov/dataportal/wp-content/uploads/2010/02/Poster-Developing-the-Solar-Model-for-the-LA-County-Solar-Mapping-Portal.pdf (last accessed 9 January 2013).

Loudat, T. 2013. The economic and fiscal effects of Hawaii's solar tax credit. https://www.novoco.com/energy/resource_files/reports/blueplanet_hawaii-solar-credit_0113.pdf (last accessed 1 November 2013).

Luque, A, and S. Hegedus. 2011. Handbook of photovoltaic science and engineering, 2nd edition. Chichester, West Sussex, U.K: John Wiley & Sons, Ltd.

Mangelsdorf, M. 2013a. Oahu's solar feeding frenzy continues. *Honolulu Civil Beat* 25 January.

Mangelsdorf, M. 2013b. Darkening skies over Hawaii solar industry. *Honolulu Civil Beat* 09 July.

Mangelsdorf, M. 2013c. Overheated market for solar energy leads to industry's painful consolidation. *Star Advertiser*. 23 October.

Marion, B, M. Andeberg, R. George, P. Gray-Hann, and D. Heimiller. 2001. PVWATTS Version 2- enhanced spatial resolution for calculating grid-connected PV performance. National Renewable Energy Laboratory presented at the NCPV Program Review Meeting Lakewood, Colorado. http://www.nrel.gov/docs/fy02osti/30941.pdf (last accessed 29 December 2013).

Maui Electric Company (MECO). 2013. Solar integration policy changes. http://www.mauielectric.com/portal/site/meco/menuitem.ed4aed221358a44973b5c410c510b1ca/?vgnextoid=0b9e9cb2ab721410VgnVCM10000005041aacRCRD&cpsextcurrchannel=1 (last accessed 20 November 2013).

National Renewable Energy Laboratory. 2012. PV WATTS Changing System Parameters. http://rredc.nrel.gov/solar/calculators/pvwatts/system.html (last accessed 20 February 2013).

National Renewable Energy Laboratory. 2013. How solar maps were made. http://www.nrel.gov/gis/solar_map_development.html (last accessed 1 December 2013).

Nguyen H, and J. Pearce. 2010. Estimating potential photovoltaic yield with r.sun and the open source geographic resources analysis support system. *Solar Energy* 84: 831-843.

Nguyen H, J. Pearce, R. Harrap, and G. Barber. 2012. The application of LiDAR to assessment of rooftop solar photovoltaic deployment potential in a municipal district unit. *Sensors* 12: 4534-4558.

North Carolina State University. 2013. Database of State Incentives for Renewables & Efficiency (DSIRE). http://www.dsireusa.org/rpsdata/index.cfm (last accessed 25 October 2013).

Pearce, J.M. 2002. Photovoltaics: A path to sustainable futures. *Futures* 34 (7): 663-674.

Perez, R, R. Seals, and A. Zelenka. 1997. Comparing satellite remote sensing and ground network measurements for the production of site/time specific irradiance data. *Solar Energy* 60: 89-96.

Perez, R, R. Seals, P. Ineichen, R. Stewart, and D. Menicucci. 1987. A new simplified version of the Perez diffuse irradiance model for tilted surfaces. *Solar Energy* 39 (3): 221-231.

Piwko, R, L. Roose, K. Orwig, M. Matsuura, D. Corbus, M. Schuerger. 2012. Hawaii solar integration study: solar modeling developments and study results. Presented at the 2nd Annual International Workshop on Integration of Solar Power in Power Systems Conference Lisbon, Portugal. 12-13 November. http://www.nrel.gov/docs/fy13osti/56311.pdf (last accessed 26 December 2013).

Redweik, P, C. Catita, and M. Brito. 2011. 3D local scale solar radiation model based on urban LiDAR data. 1749-016 Lisboa, Portugal: Faculdade de Ciências Universidade de Lisboa, Dept. Engenharia Geográfica, Geofísica e Energia.

Rich, P. 1990. Characterizing plant canopies with hemispherical photography. *Remote Sensing Review* 5: 13-29.

Rich, P, W. Hetrick, S. Saving and R. Dubayah. 1994. Using viewshed models to calculate intercepted solar radiation: applications in Ecology. http://libraries.maine.edu/Spatial/gisweb/spatdb/acsm/ac94060.html (last accessed 2 February 2013).

Robinson, D, and A. Stone. 2004. Irradiation modelling made simple: the cumulative sky approach and its application. Paper presented at: Conference on Passive and Low Energy Architecture 2004, The Netherlands: BDSP Partnership Ltd., 19-22.

Seo, D. 2010. Development of a universal model for predicting hourly solar radiation---Application: Evaluation of an optimal day lighting controller. Ph.D. dissertation, Boulder, CO: University of Colorado.

Sheng, J, J. Wilson, and S. Lee. 2009. Comparison of land surface temperature (LST) modeled with a spatially distributed solar radiation model (SRAD) and remote sensing data. *Environmental Modelling & Software* 24: 436-443.

Solar Energy Industries Association. 2011. U.S. Solar Market Insight Report Q4 2011Year in Review. http://www.seia.org/research-resources/us-solar-market-insight-report-2011-year-review (last accessed 1 December 2013).

State of Hawaii Department of Business, Economic Development and Tourism (DBEDT). 2013a. Hawaii Energy Facts and Figures June 2013. http://energy.hawaii.gov/resources/hawaii-state-energy-office-publications (last accessed 27 October 2013).

State of Hawaii Department of Business, Economic Development and Tourism (DBEDT). 2013b. Renewable EnerGIS Map. http://energy.hawaii.gov/resources/renewable-energis-map (last accessed 26 December 2013).

State of Hawaii Office of Planning. 2013. State GIS Program. http://www.state.hi.us/dbedt/gis/ (last accessed 28 October 2013).

Súri, M, and J. Hofierka. 2004. A New GIS-based solar radiation model and its application to photovoltaic assessments. *Transactions in GIS* 8:175-190.

Súri, M, T. Huld, and E. Dunlop. 2005. PV-GIS: a web-based solar radiation database for the calculation of PV potential in Europe. *International Journal of Sustainable Energy* 24: 55-67.

U.S. Energy Information Administration. 2012. Hawaii. http://www.eia.gov/state/?sid=HI (last accessed 1 February 2013).

U.S. Energy Information Administration. 2013a. Energy in Brief: What are renewable portfolio standards and how do they affect renewable electricity generation? http://www.eia.gov/energy_in_brief/article/renewable_portfolio_standards.cfm (last accessed 1 November 2013).

U.S. Energy Information Administration. 2013b. Renewable Energy Explained. http://www.eia.gov/energyexplained/index.cfm?page=renewable_home (last accessed 1 November 2013).

U.S. Energy Information Administration. 2013c. Frequently Asked Questions. http://www.eia.gov/tools/faqs/faq.cfm?id=427&t=3(last accessed 30 December 2013).

U.S. Energy Information Administration. 2013d. Solar Energy. http://www.eia.gov/energyexplained/index.cfm?page=solar_home (last accessed 25 December 2013).

U.S. Energy Information Administration. 2013e. Electric Power Monthly February 2013. http://www.eia.gov/electricity/monthly (last accessed 25 February 2013).

Voivontas, D, D. Assimacopolous, and A. Mourelatos. 1998. Evaluation of renewable energy potential using a GIS decision support system. *Renewable Energy* 13 (3): 419-427.

Western Pacific Regional Fishery Management Council. 2012. Hawaii Archipelago: Habitat and Ecosystem. http://www.wpcouncil.org/hawaii-habitat.html (last accessed 13 April 2013).

Western Region Climate Center. 2012. Climate of Hawaii. http://www.wrcc.dri.edu/ (last accessed 27 June 2013).

Wiginton, L, H. Nguyen, and J. Pearce. 2010. Quantifying rooftop solar photovoltaic potential for regional renewable energy policy. *Computers, Environment and Urban Systems* 34: 345-357.

Wilson, J. and J. Gallant. 2000. Secondary topographic attributes. In *Terrain Analysis: Principles and Applications* ed. J.P. Wilson, and J. C. Gallant, 87-131. New York: John Wiley & Sons.

Zekai, S. 2004 Solar energy in progress and future research and trends. *Progress in Energy and Combustion Science* 30 (4): 367-416.